Virus adhesion to archetypal fomites: A study with human adenovirus and human respiratory syncytial virus

Revised version submitted for consideration as a publication in the *Chemical Engineering Journal*

Xunhao Wang and Volodymyr V. Tarabara *

Department of Civil and Environmental Engineering, Michigan State University, East Lansing, MI 48824, USA

August 10, 2021

(original version submitted on April 13, 2021)

*Corresponding author: Phone: +1 (517) 432-1755; Email: tarabara@msu.edu

Abstract

Adhesion of two viruses – one enveloped (human respiratory syncytial virus, HRSV) and one non-enveloped (human adenovirus 5, HAdV5) – to four fomites (silica, nylon, stainless steel, polypropylene) was quantified and interpreted based on physicochemical properties of viruses and fomites. The selected fomites are tentatively identified as “archetypes” representing groups of materials distinctly different in mechanisms of their interfacial interactions. The surfaces are typified on the basis of their surface energy components including the dispersive (Lifshitz-van der Waals) component and two polar (electron donor and electron acceptor) components. Virus-fomite interactions are predicted using the extended Derjaguin-Landau-Verwey-Overbeek (XDLVO) theory and are experimentally assessed in tests with quartz crystal microbalance with dissipation (QCM-D). Polar interactions (manifested as hydrophobic attraction for all virus-fomite pairs but HAdV5/silica) governed virus attachment to fomites from a solution of high ionic strength typical for a respiratory fluid, while dispersive interactions played a relatively minor role. For both HAdV5 and HRSV, the areal mass density of deposited viruses correlated with the free energy of virus-fomite interfacial interaction in water, ΔG_{vwf}. The dependence of virus-fomite attachment probability on ΔG_{vwf} collapsed into one trend for both HAdV5 and HRSV pointing to the possibility of using ΔG_{vwf} as a predictor of virus adhesion. Fomite rinsing with DI water resulted in a partial virus removal attributable to longer range repulsive electrostatic interactions. The proposed methodology can guide screening and selection of materials that discourage virus adhesion. The information on the efficiency of virus attachment to

materials as a function of their surface energy components can help design anti-adhesive surfaces, develop surface cleaning solutions and protocols, and inform transport and fate models for viruses in indoor environments.

Keywords: adenovirus; respiratory syncytial virus; adhesion; QCM-D; XDLVO; surface energy

1. Introduction

Fomites are any inanimate surfaces that, when contaminated with pathogenic microorganisms, can serve as a means of transferring the pathogens to a new human host. There is growing evidence that fomites play an important role in the spread of viruses [1-3]. Higher probability of transfer is associated with fomites in indoor environments such as classrooms, hospitals, nursing homes, cruise ships, and restaurants and especially with surfaces that are frequently touched (e.g. doorknobs, refrigerator handles, dishcloths, faucets) or facilitate virus transmission through other uses (e.g. airducts, hospital linen) [3-11]. Personal protection equipment such as rubber gloves, N95 particulate respirators, surgical masks, gowns may also act as fomites for

viral cross-infection [12]. Indoor airflow may enhance transport of virus and virus-laden particles, which could be sucked into the ventilation system through return vents [13].

The COVID-19 pandemic highlighted the importance of understanding the relative importance of a various pathways for pathogen transmission. While it appears that airborne transport is the dominant mechanism for the transmission of SARS-CoV-2, indirect transmission via fomites does contribute to the spread of this virus [14-18]. Indeed, viable SARS-CoV-2 virus has been found on many surfaces and objects contaminated by respiratory secretions or droplets expelled by infected individuals [19-26]. Even if the probability of transfer on a single touch is low, high persistence of viruses on a surface translates into a higher number of touches and a higher overall infection risk [26]. A number of studies have shown that respiratory pathogens are capable of surviving on fomites for extended periods of time - from hours to months [2, 27, 28]. While the knowledge of SARS-CoV-2 transmission mechanisms is still incomplete, fomites have been firmly established as a transfer route for many other viral pathogens of significant concern to human health including influenza virus [29, 30] and norovirus [31, 32]. There is a large and growing knowledge base on the persistence of viruses at various surface [33]; at the same time, physicochemical bases of virus attachment to and removal from surfaces under different conditions remain relatively unexplored [1, 33]. Given the operational definition of risk as a product of availability and infectivity, adhesion and removal studies are needed to quantify the contribution of surface-meditated transmission to the availability term – that is the likelihood that a

particular fomite surface has an attached virus that can be detached and transmitted to a human host.

In their recent review, Castaño et al. [1] described how separate virus-fomite interactions are accounted by the classical DLVO and XDLVO theories. There have been many studies that applied XDLVO modeling to describe virus adhesion to various surfaces including membrane filters [34], iron oxide particles [35], personal care products [36], foods and food-contact surfaces [37], polyelectrolyte multilayers [38] and sand [39]. Experimental techniques used to study virus attachment to surfaces range from simple direct contact tests and traditional adsorption studies to record kinetics and isotherms of adsorption [37] to more complex methods such as those employing sensors based on surface plasmon resonance (SPR) [40] and quartz crystal microbalance [38, 41]. SPR is a powerful surface sensing technique especially suitable for studying interfacial kinetics and affinity characterization. SPR is sensitive to the vertical position of individual viruses and, coupled with microscopy, enables high-throughput imaging of single viruses [42]. Liu et al. recently employed plasmonic imaging technology to study the interfacial dynamics of SARS-CoV-2 pseudovirus (SARS-CoV-2 surrogate) adsorption on self-assembled monolayers with amino and carboxyl terminal groups from solutions including artificial saliva, artificial lung fluid and surface water [40]. SPR-based techniques are limited by the requirement of having a noble metal substrate to excite the plasmon resonance. Free of this constraint, QCM-D method has been used to explore virus adhesion to various surfaces while providing (through the dissipation data) additional information on the rheology of the adsorbed

layers. Studied surfaces include silica [41], natural organic matter [43, 44], polyelectrolyte multilayers [38], household paints [45] and self-assembled monolayers [46]. Yet, to our knowledge neither XDLVO nor QCM-D prior studies had focused on fomites with the specific goal of exploring virus adhesion to common indoor surfaces. The dearth of systematic knowledge in this area is likely due to the sheer diversity of fomites in terms of their chemical makeup, morphology and physicochemical properties of their surface. Viruses too, differ significantly in their size, charge, hydrophobicity and morphology. The broad range of possible deposition, attachment and resuspension scenarios adds to this complexity. Once viruses are attached, their survival on fomites depends on virus type, strain and inoculation titer; as a broad example, enteric viruses (which are mostly non-enveloped) are known to maintain their infectivity for longer that respiratory viruses (mostly enveloped). While a reductionist approach with its incremental accumulation of data based on studies of specific virus-fomite pairs is certainly possible, it would be desirable to identify a limited range of representative fomites, viruses and deposition conditions that can typify practically relevant scenarios and help reach generalizable conclusions.

The practical goal of the present work is to develop an approach for reducing the complexity of the broad range of surface chemistries and morphologies presented by fomites to a relatively small subset of “archetype” surfaces. An “archetype” is operationally defined as representing a set of surface properties that are characteristic of a distinct group of materials and define their adhesive behavior with respect to a virus of concern. The practical value of the approach is in facilitating both the selection of

surfaces with desired virus adhesion characteristics and the design of surface cleaning solutions and protocols. With the premise that fomites can be grouped based on the values of their surface energy components, we select four specific materials - silica, stainless steel, nylon, and polypropylene - and rationalize the selection using the van Oss theory, a three-component model for surface energy [47]. SiO_2 represents high surface energy metal oxides with a dominant electron donor component, nylon 6,6 typifies monopolar polymer with strong dispersive interactions, stainless steel is a pure metal coated by an oxide-rich passivation film with commensurate electron donor and electron acceptor components, while polypropylene represents low surface energy apolar polymers with weak dispersive interactions only.

The study employs two pathogenic microorganisms - human respiratory syncytial virus (HRSV) and human adenovirus 5 (HAdV5) - as representatives of enveloped and nonenveloped viruses, respectively. HRSV and HAdV5 are selected based on the high relevancy of both viruses for public health, demonstrated importance of fomites for their transmission, as well as for practical reasons (both are available commercially in high purity and titer). HAdV, a large nonenveloped virus [48, 49], is highly resistant to both monochloramine and UV irradiation [50] and can survive on fomites for many days [2]. HAdV is primarily spread by the fecal-oral and respiratory routes through person-to-person contact and fomite-mediated transfer [51, 52]. Adenoviruses can cause a range of clinical diseases, including respiratory, gastrointestinal, and conjunctival illness. HRSV, which features a distribution of sizes and morphologies (spherical or filamentous) [53], can cause severe disease, especially in children, the elderly and

immunocompromised adults [54]. HRSV is primarily spread by large droplets and via fomites, and can survive on nonporous surfaces, skin, and gloves for many hours [55, 56]. The makeup of the solution from which deposition occurs affects the likelihood of virus attachment. A large number of illnesses are associated with more than 150 different types of pathogenic respiratory viruses transmittable from bodily secretions to surfaces. Indeed, viruses deposit onto fomites either as a result of direct contact with an infected human or from respiratory droplets produced by such person. Given that both HRSV and HAdV5 are present in the human respiratory tract, the present study focuses on the latter transmission route and explores virus deposition from a high ionic strength electrolyte (150 mM NaCl) typical for respiratory fluid (9 $g \cdot L^{-1}$, physiological concentration [57]). While the composition of respiratory fluid is complex and varies with individual's health status [58, 59], some aggregate characteristics such as pH and ionic strength can be captured in modeling studies.

The study explores the hypothesis that virus attachment to fomites in a high ionic strength solution is governed by hydrophobic interactions. To test the hypothesis, we use quartz crystal microbalance with dissipation (QCM-D) and QCM-D sensors with specialty coatings to experimentally determine attachment efficiency for HRSV and HAdV5 depositing onto four "archetypal" fomites that span a range of hydrophobicities. The experimental measurements are complemented by modeling based on the extended Derjaguin-Landau-Verwey Overbeek (XDLVO) theory. Experimental and modeling results are interpreted in terms of polar, dispersive, and electrostatic interactions between viruses and fomites.

2. Materials and Methods

2.1 Reagents, fomites, viruses

All chemical reagents were of high purity (>99%). NaCl, KCl, glycerol, sodium dodecyl sulfate (SDS), ethylene glycol (EG) and diiodomethane (DID) were purchased from Sigma Aldrich. QCM-D sensors coated with materials representing fomites – silica, nylon 6,6 (hereafter “nylon”), stainless steel (SS), and polypropylene (PP) – were purchased from Nanoscience. Deconex 11 (Fisher Scientific) was used as the cleaning solution for PP and nylon sensors (see Supplementary Material (SM)). Silica and SS sensors were cleaned with 2% SDS solution and Hellmanex II (Hellma GmbH & Co. KG), respectively.

Human adenovirus 5 (HAdV5) was purchased from American Type Culture Collection (ATCC® VR-1516™) [60]. The product is an aqueous suspension of HAdV5 in 20 mM TRIS, 25 mM NaCl, 2.5% glycerol (pH 8.0) [61] purified by single column chromatography [62]. HAdV5 is a non-enveloped dsDNA virus with an icosahedral nucleocapsid. Human respiratory syncytial virus (HRSV; strain: Long) was also purchased from ATCC (VR-26PQ™) [63]. The product is an aqueous suspension of HRSV in 50 mM Tris-HCl, 150 mM NaCl, 1 mM EDTA prepared by concentrating another HRSV stock (ATCC VR-26™) via sucrose cushion centrifugation [64]. HRSV is

an ssRNA virus with a helical nucleocapsid surrounded by matrix protein and an envelope. Spherical and filamentous HRSV virions have been identified [53, 65, 66].

2.2 Virion characterization: Hydrodynamic size, ζ-potential, concentration

Electrophoretic mobility and hydrodynamic diameter of HRSV virions were measured by laser doppler micro-electrophoresis (Zetasizer Nano ZS, Malvern) and dynamic light scattering (DLS), respectively. The 1 mM KCl diluent used in these measurements was pre-filtered through 0.22 µm syringe filter. The charge and size of HAdV5 (ATCC® VR-1516™) were determined previously [36]. These measurement techniques capture averaged values of virus charge and size. While the electrical charge has a certain distribution over the virus surface, streaming potential is an aggregate estimate of the surface potential averaged over the surface. Similarly, DLS estimates particle's diffusion coefficient, which is then converted to particle size assuming that the particle is spherical. Yet viruses (including HAdV5 [36] and HRSV [53, 65, 67]) have complex morphology. The adopted approach where viruses are treated as spherical colloids with a chemically homogenous surface are justified as both XDLVO modeling (section 2.4) and interpretation of experimental data on virus adhesion obtained by QCM-D (sections 2.5 and 3.1) rely on these assumptions. As a complement to DLS measurements, both HRSV and HAdV5 were imaged using transmission electron microscopy (TEM, JEM-1400 Flash, Jeol, Nieuw-Vennep). TEM sample preparation and imaging procedures are described in SM, section S1. Virus concentration was measured by fluorometry

(Qubit fluorometer, Invitrogen) with Qiagen DNA and RNA mini kits used to extract dsDNA from HAdV5 and ssRNA from HRSV. The ssRNA High Sensitivity and dsDNA High Sensitivity modes were utilized for HRSV and HAdV5 genome quantification, respectively.

2.3 Quantifying surface energy of viruses and fomites

2.3.1 Approach

Hydrophobicity of a solid (s) can be quantified in terms of the free energy of its interfacial interaction with an identical material when immersed in water (w), ΔG_{sws} [47]. We applied this approach to evaluate hydrophobicity of viruses (v) and fomites (f) by computing ΔG_{vwv} and ΔG_{fwf}, respectively. The calculation relies on the knowledge of the solid's surface energy in terms of its three components: two Lewis acid-base (electron acceptor, γ_s^+, and electron donor, γ_s^-) components and the Lifshitz-van der Waals component, γ_s^{LW}. The Lewis acid-base components are also described as *polar* while the Lifshitz-van der Waals component is often referred to as *dispersive* or *apolar*. The components can be determined by measuring contact angles (θ) of three probe liquids (l) with known γ_l^{LW}, γ_l^+ and γ_l^- on the surface of the solid and substituting these values into the Young-Dupré equation [68, 69]

$$(1 + cos\theta)\gamma_l^{TOT} = 2\left(\sqrt{\gamma_s^{LW}\gamma_l^{LW}} + \sqrt{\gamma_s^+\gamma_l^-} + \sqrt{\gamma_s^-\gamma_l^+}\right), \quad (1)$$

where γ_l^{TOT} is the total surface energy of the probe liquid:

$$\gamma^{tot} = \gamma^{LW} + \gamma^{AB} = \gamma^{LW} + 2\sqrt{\gamma^-\gamma^+}. \quad (2)$$

The free energy of solid-solid interfacial interaction in water is given by

$$\Delta G_{sws} = -2\left(\sqrt{\gamma_s^{LW}} - \sqrt{\gamma_w^{LW}}\right)^2 - 4\left(\sqrt{\gamma_s^+\gamma_s^-} + \sqrt{\gamma_w^+\gamma_w^-} - \sqrt{\gamma_s^+\gamma_w^-} - \sqrt{\gamma_s^-\gamma_w^+}\right) \quad (3)$$

where γ_w^{LW}, γ_w^+ and γ_w^- are surface energy components of water. A positive value of ΔG_{sws} indicates a hydrophilic surface, while negative ΔG_{sws} corresponds to a hydrophobic surface. The absolute value of ΔG_{sws} indicates the degree of hydrophilicity (or hydrophobicity, when $\Delta G_{sws} < 0$) of the surface. As in the case with size and charge measurements, the determination of virus and fomite surface energies based on contact angles of probe liquids treats these surfaces as chemically homogeneous. Thus, the presence of hydrophobic or hydrophilic “patches” on a surface is not accounted for and energy values describe interaction of “equivalent” chemically homogenous surfaces.

2.3.2 Experiments

Contact angles of three probe liquids - DI water, glycerol, and DID - on fomite surfaces and HRSV lawns were measured using the sessile drop method (goniometer / tensiometer model 250, ramé-hart). Additional contact angle measurements with EG as the fourth probe liquid were done for the polypropylene surface. Virus lawns were

formed by filtering virus stock suspensions through a polyethersulfone ultrafiltration membrane (50 kDa, Pall Life Sciences) to form a multilayer (> 5 monolayers) cake, or lawn, of virions [70]. Prior to recording contact angle values, the lawn was allowed to dry in air until the contact angle of water on the virus lawn stabilized. A separate set of measurements was performed to study the effect of pH and ionic strength on water contact angles on fomite surfaces. All measurements were performed in the air at the ambient temperature of 22 °C and the relative humidity of 47 %. The droplet volume was 6 µl. Contact angle values were calculated by DROPimage Advanced software based on recorded droplet shapes.

2.4 Modeling virus-fomite interactions. Extended Derjaguin-Landau-Verwey-Overbeek theory

The interactions between colloidal and surfaces can be predicted by XDLVO theory. The theory describes the total energy of interaction U_{vwf}^{XDLVO} between a spherical particle (representing a virus (v)) and a flat surface (representing a fomite (f)) in water (w) as a sum (see eq. (7)) of Lifshitz-van der Waals (LW), U_{vwf}^{LW}, electrostatic double layer (EL), U_{vwf}^{EL}, and Lewis acid-base (AB), U_{vwf}^{AB}, energies expressed as follows:

$$U_{vwf}^{LW}(d) = -\frac{Aa}{6d} = 2\pi d_0^2 \frac{a}{d} \Delta G_{d_0}^{LW} \quad (4)$$

$$U_{vwf}^{EL}(d) = \pi \varepsilon_r \varepsilon_0 a \left[2\psi_v \psi_f \, ln\left(\frac{1+e^{-\kappa d}}{1-e^{-\kappa d}}\right) + \left(\psi_v^2 + \psi_f^2\right) ln(1-e^{-2\kappa d}) \right] \quad (5)$$

$$U_{vwf}^{AB}(d) = 2\pi a\lambda\Delta G_{d_0}^{AB}\, exp\left(\frac{d_0 - d}{\lambda}\right) \quad (6)$$

$$U_{vwf}^{XDLVO} = U_{vwf}^{LW} + U_{vwf}^{EL} + U_{vwf}^{AB} \quad (7)$$

where a is the virus radius, d is the virus-fomite minimal interfacial separation distance, $A = -12\pi d_0^2 \Delta G_{d_0}^{LW}$ is the Hamaker constant, ε_r is the relative dielectric permittivity of water (for water at 25 °C, $\varepsilon_r \approx 78.3$), ε_0 is the dielectric permittivity of vacuum (ε_0 = 8.854×10^{12} C·V^{-1}·m^{-1}), ψ_v and ψ_s are surface potentials of the virus and fomite, respectively, κ is the inverse Debye screening length, λ is the characteristic delay length of AB interactions in water (λ = 0.6 nm), and d_0 is the minimum separation distance (d_0 = 0.158 nm) due to Born repulsion. Surface potentials ψ_v and ψ_f are commonly approximated by ζ-potentials (ζ_v and ζ_f). Values of $\Delta G_{d_0}^{LW}$ and $G_{d_0}^{AB}$ in eq. (4) and eq. (6) are given by:

$$\Delta G_{d_0}^{LW} = 2\left(\sqrt{\gamma_v^{LW}} - \sqrt{\gamma_w^{LW}}\right)\left(\sqrt{\gamma_w^{LW}} - \sqrt{\gamma_f^{LW}}\right) \quad (8)$$

$$\Delta G_{d_0}^{AB} = 2\sqrt{\gamma_w^+}\left(\sqrt{\gamma_f^-} + \sqrt{\gamma_v^-} - \sqrt{\gamma_w^-}\right) + 2\sqrt{\gamma_w^-}\left(\sqrt{\gamma_f^+} + \sqrt{\gamma_v^+} - \sqrt{\gamma_w^+}\right) - 2\sqrt{\gamma_f^+\gamma_v^-} - 2\sqrt{\gamma_f^-\gamma_v^+} \quad (9)$$

The free energy of virus-fomite interfacial interaction in water, ΔG_{vwf}, is

$$\Delta G_{vwf} = \Delta G_{d_0}^{LW} + \Delta G_{d_0}^{AB} \quad (10)$$

Note that eq. (3) can be obtained from eqs. (8 - 10) by substituting subscripts v and f for s. Lewis acid-base interactions are also referred to as electron donor/electron acceptor or polar interactions. Hydrophobic attraction and hydrophilic repulsion (i. e. hydration pressure) are two types of polar interactions [47].

Virion size, surface charge and surface energy components as well as surface charge and surface energy components of each of the four fomites were used as inputs to the XDLVO model. In its description of the energy of sphere-plate interaction energy, the model assumes that both surfaces are smooth. The effect of surface roughness can be taken into account by adding the sphere-asperity term to the calculation of the total interaction energy [71, 72]. Applied to the calculation of the energy of interaction between household paint coatings and human adenovirus 40 (a virus similar to HAdV5), this approach showed that the presence of ~ 27 nm asperities on paint-coated QCM-D sensors had only a minor effect (~ 10% change in the total energy) [38]. Based on the manufacturer's data, the root mean square surface roughness of QCM-D sensors is < 1 nm for stainless steel and silica and ~ 3.5 nm for nylon and polypropylene [73] – well below the 27 nm value for which XDLVO predictions were only weakly affected.

Most data were obtained in experiments as described in sections 2.2 and 2.3. Size and charge of HAdV5 were determined in our earlier study and used in the present work [36]. Values of the ζ-potential of the four fomites as a function of pH were adopted from literature (Zemljic et al. [74] for PP, Hedberg et al. [75] for SS, Zhang et al. [76] for nylon, and Wang et al. [36] for silica).

2.5 QCM-D studies of HAdV5 and HRSV attachment to fomites

2.5.1 Approach: Quantifying virus-fomite attachment efficiency

To accurately assess the mass flux of viruses towards the QCM-D sensor surface one needs to solve the Graetz problem of diffusion-limited transport to a flat plate from a crossflow [77, 78]. Given the complexity of the QCM-D chamber geometry and the need to add surface reaction (describing the finite probability of virus attachment to the sensor surface), the solution would need to be numerical. Instead, we propose a simple model that describes the rate of virus deposition (ng/min) onto QCM-D sensor surface as

$$\frac{dm_v}{dt} = \alpha_{vf} j_m A_s \tag{11}$$

where α_{vf} (unitless) is the virus-fomite attachment efficiency, A_s (cm^2) is surface area of the sensor and j_m (ng·cm^{-2}·min^{-1}) is the mass flux of viruses towards the sensor. We define mass transfer coefficient, k (m·s^{-1}), as follows:

$$j_m = k(C_b - C_s) \tag{12}$$

where C_b and C_b are virus concentrations in the bulk of the flow and at the sensor surface, respectively. For early stages of deposition $C_s \ll C_b$, the sensor is mostly virus-free and the rate of virus deposition is approximately constant:

$$\frac{dm_v}{dt} \approx \alpha_{vf} k C_b A_s \tag{13}$$

The linearity of the deposition rate dependence on concentration was confirmed in tests with different C_b (see SM, Fig. S3). Because the rate of mass transfer across the viscos sublayer at the QCM-D sensor surface depends on virus diffusivity, mass transfer coefficient, k, needs to be determined for each virus separately.

2.5.2 QCM-D experiments

The QCM-D E4 system (Biolin Scientific) was used to quantify the deposition of viruses onto sensor surfaces. Prior to measurement, QCM-D sensors were cleaned (see SM, section S4) and then mounted into the flow chamber to determine their resonance frequency in air. QCM-D tests were carried out at 25 °C in a continuous flow mode (0.15 ml/min) using a digital peristaltic pump (IPC, four channels, ISMATEC). The sensors were first equilibrated with DI water (pH 5.8), then with 0.22 μm filtered NaCl electrolyte (pH 5.8) and only after the vibration frequency stabilized were challenged with a virus suspension. Procedures performed to avoid air bubble formation on the surface of hydrophobic PP sensors are described in SM, section S2. QCM frequency and dissipation were recorded every 1 min. The frequency shifts were fitted into the Sauerbrey equation [79] to compute the change in areal mass density, Δm (ng·cm^{-2}):

$$\Delta m = -\frac{C\Delta f}{n} \tag{14}$$

where C is the mass sensitivity constant (C = 17.7 ng·Hz^{-1}·cm^{-2}), n is the overtone number and Δf is the frequency shift (Hz). All virus suspensions used in QCM-D tests

were prepared by diluting the virus stock in a background electrolyte pre-filtered through a 0.22 μm filter. Background electrolytes were either 150 mM NaCl (pH 5.8) or 1 mM NaCl (pH 4.1 in tests with HAdV5 and pH 3.8 in tests with HRSV). The 150 mM NaCl solution was used in most tests with all 8 fomite-virus pairs. The 1 mM NaCl was used in additional tests with HAdV5/PP and HRSV/PP pairs to simulate conditions of α_{vf} = 1 (see SM, section S6). Prior to use in QCM-D experiments, virus suspensions were vortexed for 15 s to ensure a uniform dispersion of virions.

After ~ 60 min of QCM-D measurement, the sample chamber and tubing were flushed with the background electrolyte followed by DI water (pH 5.8). Each sensor was used in 5 to 7 different QCM-D experiments and cleaned after each test. To ascertain that cleaning did not affect the hydrophobicity of the sensor coatings, contact angles of three probe liquids were re-measured after multiple cycles of QCM-D tests and cleaning (see SM; Tables S2 – S4).

3. Results and Discussion

3.1 Virus concentration, size, charge and hydrophobicity.

The concentrations of HAdV5 and HRSV in stock suspensions were verified by fluorometry (Qubit, Invitrogen) and found to be somewhat different from the values given by ATCC for these specific lots. The measured concentrations were 3.45×10^{11} GC/ml for HAdV5 (lower than ATCC-reported 5.8×10^{11} GC/ml [61]) and 2.65×10^{10} GC/ml for HRSV (higher than ATCC-reported 1.7×10^{10} GC/ml [64]). Based on the measured values of the hydrodynamic size (see below) and the approximate virion density, the corresponding mass concentrations of HAdV5 and HRSV in the feed suspensions were estimated to be 28 ng/mL and 12 ng/mL.

The hydrodynamic diameter, d_h, of HAdV5 was ~ 102 nm as determined by DLS in our previous study [36]. This size is derived using Stokes-Einstein equation (eq. (15)) based on the measured value of HAdV5 diffusivity, D = 4.27×10^{-12} ($m^2 \cdot s^{-1}$).

$$D = \frac{k_B T}{3\pi\mu d_h} \tag{15}$$

The difference between HAdV5 diameter values estimated from TEM images (~ 90 nm, Figures 1G and 1H) and measured by DLS is likely due to the presence of fibers on the HAdV5 surface [39, 48], which slow down diffusion.

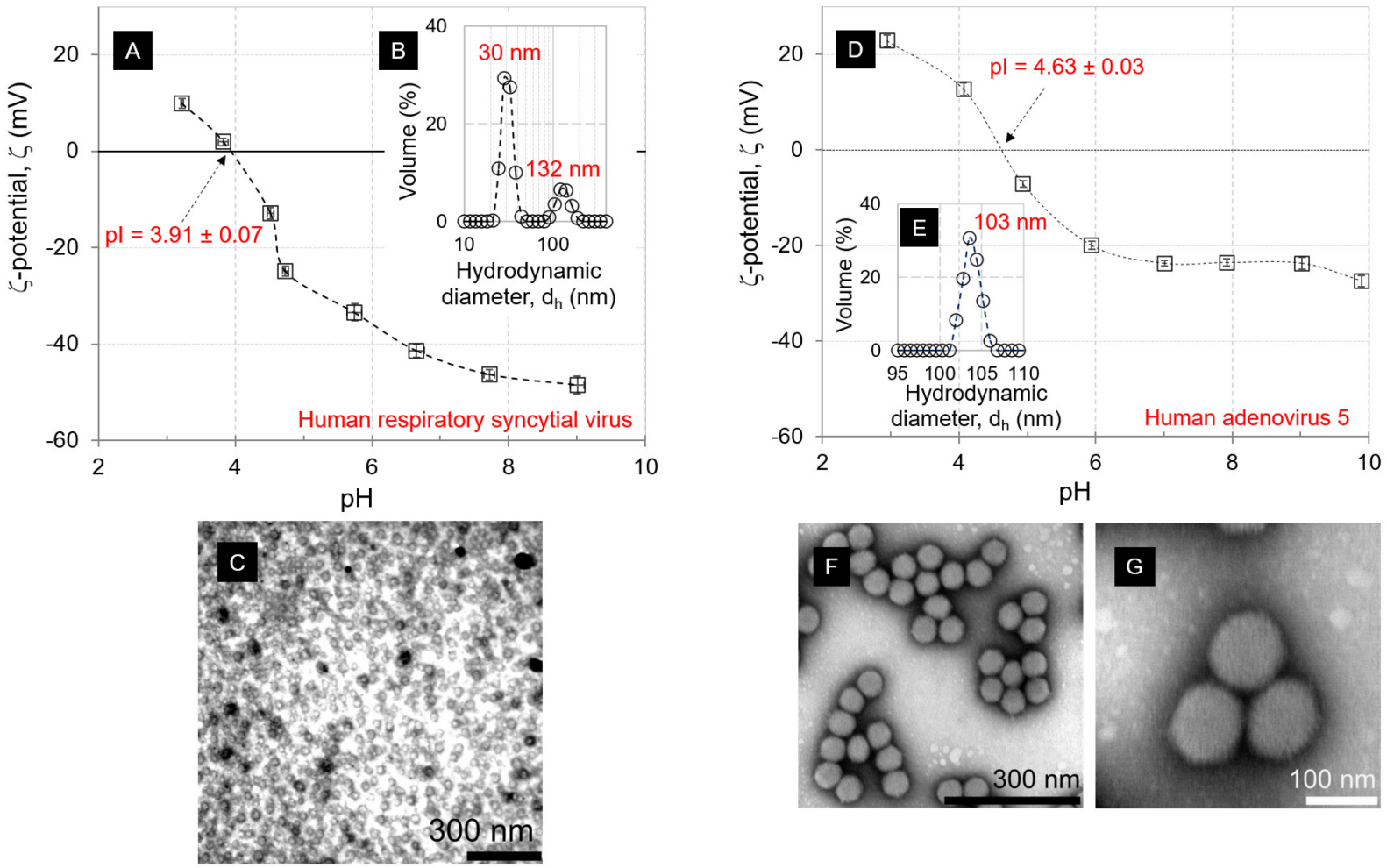

Figure 1. ζ-potential as a function of pH (A, D), size distribution (B, E), and TEM images (C, F, G) of HRSV (A-C) and HAdV5 (D-G). In A, B, D and E, lines are added to guide the eye. Charge and size values for HAdV5 (D, E) are adopted from our earlier report [36]. Additional TEM images are shown in SM, Figure S2.

Table 1. Contact angle of probe liquids, surface energy parameters (γ^{LW}, γ^{+}, γ^{-}, γ^{AB}, γ^{tot}) and the free energy of interfacial interaction in water (ΔG_{sws}) of four fomites (clean, before use) and two viruses. Error estimates were obtained by propagating experimental errors in measured contact angles through the calculation of surface energy components (eqs (1) and (2)) and ΔG_{sws} (eq. (3)). Additional contact angle measurements were performed for the four fomites using 150 mM NaCl solution at pH 5.8; the contact angle data and calculated surface energy values are given in SM (Table S2).

Parameter			Fomites				Viruses	
			Silica	Nylon	Stainless steel	Polypropylene	HAdV5 [B]	HRSV [C]
Contact angle		H_2O [A]	12.1 ± 0.9	50.1 ± 1.4	60.7 ± 1.9	100.5 ± 1.5	72.3 ± 0.4	73.5 ± 2.6
		Glycerol	14.7 ± 1.5	50.5 ± 1.0	31.4 ± 0.8	89.4 ± 1.6	70.5 ± 1.2	63.6 ± 1.3
		DID	31.4 ± 2.6	12.4 ± 0.9	50.2 ± 1.5	58.6 ± 2.9	28.5 ± 1.0	45.2 ± 2.0
		EG	n/a	n/a	n/a	77.5 ± 1.8	n/a	n/a
Surface energy	($mJ \cdot m^{-2}$)	γ^{LW}	43.6 ± 1.1	49.6 ± 0.2	34.2 ± 0.8	29.4 ± 1.7	36.1 ± 1.9	36.9 ± 1.1
		γ^{+}	2.2 ± 0.2	0.02 ± 0.02	6.8 ± 0.5	0	0	0.4 ± 0.2
		γ^{-}	44.5 ± 0.7	26.9 ± 2.1	7.4 ± 1.5	0.5 ± 0.2	14.9 ± 1.2	9.0 ± 2.6
		γ^{AB}	19.7 ± 0.6	1.4 ± 0.4	14.2 ± 1.6	0	0	3.8 ± 1.1
		γ^{tot}	63.3 ± 1.2	51.0 ± 0.4	48.4 ± 1.8	29.4 ± 1.7	36.1 ± 1.9	40.7 ± 1.5
		ΔG_{sws}	15.7 ± 1.1	- 8.5 ± 3.9	- 25.5 ± 2.9	- 88.9 ± 2.5	- 27.7 ± 1.1	- 40.2 ±

Notes: [A] DI water, pH 5.8; [B] Wang et al. [36]; [C] Contact angle measurements were performed on top of a multilayer lawn of viruses assembled, by filtration, on the surface of a hydrophilic (ΔG_{sws} = 18.9 mJ·m^{-2}) polyethersulfone ultrafiltration membrane.

In addition, drying-induced shrinkage of virions during negative staining may have decreased the diameters observed in TEM images [80]. A similar discrepancy between DLS- and TEM-derived sizes was also reported for HAdV40 [81]. For the HRSV suspension, the volume-based particle size distribution obtained by DLS (Fig. 1B; note the logarithmic size scale) was bimodal with a larger peak at ~ 30 nm and a smaller peak at ~ 132 nm, indicating varied particle size or morphology of HRSV [53, 65, 67]. Given that volume-based distributions are sensitive to the presence of larger particles, the small intensity of the 132 nm peak points to their low abundance. Still, because deconvolution of DLS scattered light frequency data assumes monodisperse scatterers, multimodal distributions should be treated with caution as quantitatively inaccurate. In such case, direct visualization by TEM is especially valuable. TEM imaging showed the preponderance of smaller and spherical HSRV virions (Fig. 1C) although larger and irregularly shaped virions were also occasionally observed. The latter observation is consistent with earlier reports of HRSV polymorphism [53, 65, 67].

Based on the measured values of HRSV electrophoretic mobility as a function of pH (Fig. S1), the isoelectric point (pI) of HRSV was estimated to be 3.91 ± 0.07. Electrophoretic mobilities were converted to ζ-potentials (Fig. 1A) using Ohshima

equation [82] (see SM, section S5, Table S1). The Ohshima approach was used because for HRSV in 1 mM KCl, $\kappa a \approx 6.4$, making neither Smoluchowski expression (valid when $\kappa a \gg 1$) nor Hückel expression (valid when $\kappa a \ll 1$) applicable. At pH 5.8, which has been reported to fall within the pH range typical for human respiratory fluid [83], the ζ-potential of HRSV is - 33.9 ± 2.6 mV. The electrophoretic mobility of HAdV5 was measured earlier [36]; the pI of HAdV5 is 4.6 ± 0.03 while ζ-potential at pH 5.8 is - 18.2 ± 0.1 mV (Fig. 1D).

Hydrophobicity of adenoviruses is responsible for their low recoveries from water [84-86] presumably in relation to virus loss to surfaces during sample handling (e. g. storage, transfer, sample concentration) [81]. The high negative values of ΔG_{sws} reported for HAdV40 (- 30.4 mJ·m^{-2} [81]) and HAdV5 (- 27.7 mJ·m^{-2} [36]) confirm their hydrophobicity. The propensity of these viruses to attach to surfaces also implies a higher likelihood of fomite-mediated transfer. In the present work, HRSV was determined to be even more hydrophobic (than HAdV5 and HAdV40) with ΔG_{sws} of - 40.2 mJ·m^{-2}. In terms of surface energy components, the hydrophobicity of HAdV40, which is a monopolar virus ($\gamma^+ = 0$; Table 1), was due to the small value of the only non-zero component of virus-water polar interactions, $\sqrt{\gamma_s^- \gamma_w^+}$, when compared to the polar interaction between water molecules, $\sqrt{\gamma_w^+ \gamma_w^-}$ (see eq. (3)). The latter term represents the hydrogen bonding energy of the cohesion of water. To our knowledge the present study is the first report of HRSV surface energy and, more generally, of HRSV hydrophobicity.

3.2 Fomite hydrophobicity

In the order from most hydrophilic to most hydrophobic, the four fomites ranked as follows: silica > nylon > SS > PP, with ΔG_{fwf} values of 15.7, - 8.5, -25.5, and - 88.9 mJ·m^{-2}, respectively (Table 1). These estimates were computed based on contact angles measured using DI water at pH 5.8 as one of the probe liquids. For PP, $\sqrt{\gamma_s^+}$ took on a small negative value; this is a common observation for monopolar or near-monopolar materials where an experimental error prevents solving eq. (1) to determine surface tension components of the solid [87]. In this study, we assumed that γ_s^+ for PP is zero and computed γ_l^- using a graphical approach described by McCafferty [88] (see SM, section S8).

Surfaces in contact with aqueous solutions are most hydrophobic at pH near the pI of the surface. Indeed, isoelectric points can be determined by contact angle titration [89]. Cuddy et al. [90] performed such measurements for several common QCM-D sensors (Al_2O_3, Au, SiO_2, Ag, Ti). Because pH of the deposition and cleaning solutions can vary, it is important to evaluate hydrophobicity of fomites at different pH. The pH dependence of ΔG_{fwf} for each fomite is shown in Fig. 2. The trends closely followed those of water contact angles (Fig. S4). For all four fomites the dependence of ΔG_{fwf} on pH was a curve with a minimum. The dependence was strongest for stainless steel, which was considerably hydrophobic (ΔG_{fwf} = - 24.2 mJ·m^{-2}) near its pI but became hydrophilic (ΔG_{fwf} > 0) at pH $\lesssim$ 2.1 and pH $\gtrsim$ 8.4. Hydrophobicity of nylon, PP, silica and SS

peaked at pH of ~ 2.5, 2.6, 3.9 and 4.0 respectively. The estimate for silica is in good agreement with the pI value determined for silica-coated QCM-D sensors by Cuddy et al. [90].

Virga et al. [91] showed that the contact angle of an aqueous electrolyte is a stronger function of pH for higher ionic strength electrolytes. For the solutions employed in this work (DI water, 1 mM NaCl, 150 mM NaCl), the effects of the ionic strength of the contact angle (Fig. S4) and, by extension, hydrophobicity (Fig. 2) were not statistically significant. It was also assumed that the dependence of the surface tension of the aqueous solution on its ionic strength and pH was insignificant. Indeed, for the electrolyte used in the present work (150 mM NaCl) the effect was reported to be small: ~ 2 mJ·m^{-2} increase over the surface tension of DI water [92].

3.3. Quantifying virus-fomite interactions. Four archetypal fomites

Table 2 presents values of ΔG_{vwf} and its dispersive and polar constituents ($\Delta G_{d_0}^{LW}$ and $\Delta G_{d_0}^{AB}$, see eqs (8-10)) for all eight virus-fomite pairs. The net interfacial interaction is attractive ($\Delta G_{vwf} < 0$) for all pairs except HAdV5/silica. A detailed analysis of ΔG_{vwf} in terms of surface energy components (i. e. relative contributions of various terms in eqs. (8) and (9)) can identify surface properties responsible for the strength, or weakness, of

the overall interaction. Potentially, such analysis can help with the selection of surfaces resisting virus adhesion as well as the optimal makeup of surface cleaning solutions.

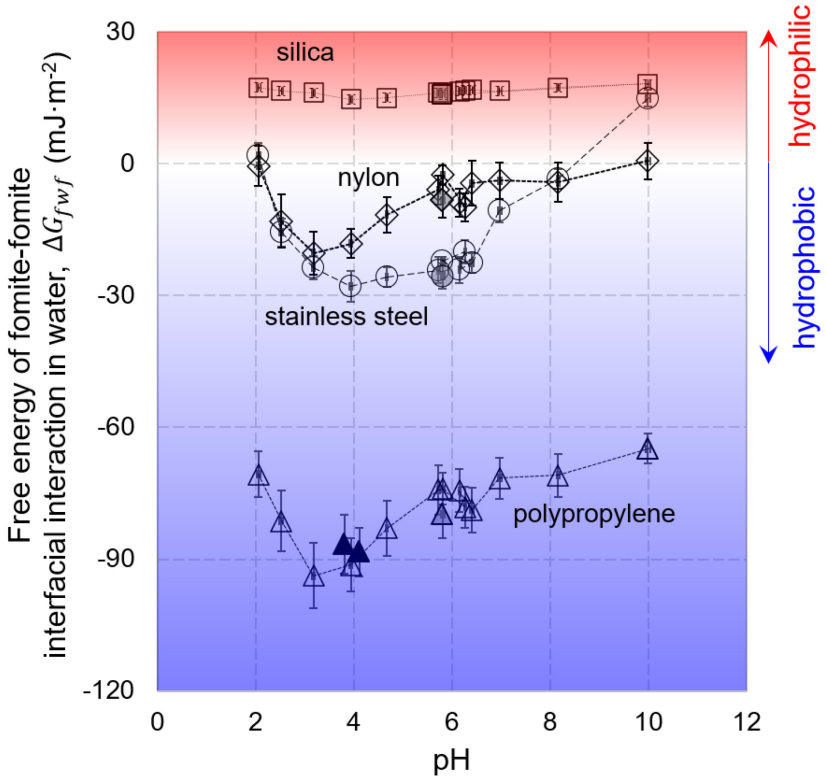

Figure 2. Free energy of interfacial interaction in water (ΔG_{fwf}) of four fomites as a function of pH. Depending on the type of aqueous solution used as a probe liquid, values are shown using either empty symbols (150 mM NaCl at pH 5.8; Table S1) or gray symbols (DI water at pH 5.8; Table 1) or black symbols (1 mM NaCl water at pH 3.8 and 4.1; Table S5).

Table 2. Free energy of virus-fomite interfacial interaction in water, ΔG_{vwf}, and its dispersive ($\Delta G_{d_0}^{LW}$) and polar ($\Delta G_{d_0}^{AB}$) components, for eight different virus-fomite pairs. Standard deviations were obtained by propagating experimental errors in measured contact angles (Table 1) through the calculation of surface energy parameters (eqs. (1) and (2)) and ΔG_{vwf} (eqs. (8), (9), and (10)).

Virus	Fomite	Interaction energy (mJ·m^{-2})		
		$\Delta G_{d_0}^{LW}$	$\Delta G_{d_0}^{AB}$	ΔG_{vwf}
Human respiratory syncytial virus	Silica	- 5.5 ± 0.4	- 0.4 ± 3.2	- 5.8 ± 3.2
	Nylon	- 6.7 ± 0.4	- 19.0 ± 1.8	- 25.7 ± 1.9
	Stainless steel	- 3.3 ± 0.3	- 30.6 ± 3.3	- 33.9 ± 3.2
	Polypropylene	- 2.1 ± 0.5	- 59.1 ± 4.6	- 61.3 ± 4.6
Human adenovirus 5	Silica	- 5.2 ± 0.6	7.9 ± 1.1	2.7 ± 1.3
	Nylon	- 6.4 ± 0.8	- 10.4 ± 0.0	- 16.7 ± 0.8
	Stainless steel	- 3.2 ± 0.4	- 29.4 ± 0.8	- 32.5 ± 0.9
	Polypropylene	- 2.0 ± 0.5	- 56.0 ± 0.0	- 58.0 ± 0.5

A common feature for all four fomites and the two viruses studied in this work is that their γ^{LW} component is higher than that of water (γ_w^{LW} = 21.8 mJ·m^{-2}); as a result, for none of the virus-fomite pairs the conditions ($\gamma_f^{LW} < \gamma_w^{LW} < \gamma_v^{LW}$ or $\gamma_v^{LW} < \gamma_w^{LW} < \gamma_f^{LW}$) necessary for dispersive interaction to be repulsive ($\Delta G_{d_0}^{LW} > 0$; eq. (8)) were fulfilled.

Thus, for both HAdV5 and HRSV their dispersive interactions with each of the four fomites were attractive. Notably, some common materials such as PTFE (γ_w^{LW} = 18.6 mJ·m^{-2}; see Table 2.3 in the book by Kinloch [93]) would have repulsive dispersive interactions with HAdV5 and HRSV in water.

In several other respects, the four selected fomites differed. In what follows, the differences are described and presented as the basis for considering the four fomites as typifying distinct groups of materials (i. e. as “archetypes”).

1. *Silica* is characterized by a large electron donor component of its surface tension such that $\gamma_f^- \gg \gamma_f^+$. Silica’s polar interactions with HAdV5 are repulsive due to hydration of both silica and virus surfaces (large $\gamma_f^-\gamma_w^+$ and $\gamma_v^-\gamma_w^+$ terms in eq. (9)). Repulsive polar interactions ($\Delta G_{d_0}^{AB} > 0$) are referred to as *hydration pressure*. For the HAdV5/silica pair, hydration pressure overcomes water cohesion given by $\gamma_w^-\gamma_w^+$ so that even in the presence of attractive dispersive forces ($\Delta G_{d_0}^{LW} < 0$), the overall interaction is a mild repulsion ($\Delta G_{vwf} > 0$).
2. *Nylon* is less polar than silica. A near-monopolar surface ($\gamma_f^+ \cong 0$), nylon also has a smaller γ_f^-. As a result, the electron-donor attraction between nylon and viruses is weaker than water cohesion leading to $\Delta G_{d_0}^{AB} < 0$. Attractive polar interactions ($\Delta G_{d_0}^{AB} < 0$) are referred to as *hydrophobic attraction*. In case of nylon, the attraction is further enhanced due to the high (the highest among the four fomites) dispersive component of nylon’s surface tension, γ_f^{LW}.

3. *Stainless steel* surface has a substantial electron acceptor component such that $\gamma_f^+ \cong \gamma_f^-$. This gives stronger polar interactions with viruses (i. e. higher $\gamma_f^+\gamma_v^-$ and $\gamma_f^-\gamma_v^+$). Notably, these terms are independent of the properties of the continuous phase.
4. *Polypropylene* is an apolar material ($\gamma_f^+ \cong 0$; $\gamma_f^- \cong 0$). Because the dispersive component of PP's surface tension, γ_f^{LW}, is close to that of water (29.4 vs 21.8 mJ·m^{-2}; Table 1), dispersive interactions of PP with any virus are also weak (eq. (8)). For viruses such that $\gamma_v^{LW} > \gamma_w^{LW}$ (which is the case for both HRSV and HAdV5), the dispersive interactions are attractive. As a result, hydrophobic attraction is the dominant mechanism of virus interaction with PP surface.

Many common materials are monopolar or nearly so with γ_f^+ very close to zero [94]. For such materials, substituting eq. (8) and eq. (9) into eq. (10), and posing ΔG_{vwf} = 0, gives the following relationship between γ_f^- and γ_f^{LW}:

$$\gamma_f^- = \left[\frac{\sqrt{\gamma_v^{LW}\gamma_w^{LW}} + \sqrt{\gamma_f^{LW}\gamma_w^{LW}} - \sqrt{\gamma_v^{LW}\gamma_f^{LW}} - \gamma_w^{LW} - 2\sqrt{\gamma_w^-\gamma_w^+} + \sqrt{\gamma_w^-\gamma_v^+} + \sqrt{\gamma_w^+\gamma_v^-}}{\sqrt{\gamma_v^+} - \sqrt{\gamma_w^+}}\right]^2 \quad (16)$$

In the 2D space with γ_f^- and γ_f^{LW} as coordinates, eq. (16) corresponds to the boundary separating all monopolar materials into those that have an overall attractive interaction (ΔG_{vwf} < 0) and those having an overall repulsive interaction (ΔG_{vwf} > 0) with a given

colloid. Figure 3 illustrates such boundary for the case when the colloid is HRSV[1]. Both the monopolar PP and the near-monopolar nylon (Table 1) interact with HRSV favorably. Note that ΔG_{vwf} does not account for electrostatic interactions, which, under appropriate conditions (see section 3.5), can create a substantial primary barrier and prevent adhesion. Such graph constructed for a given virus with known surface tension components would allow screening of various candidate materials and selecting ones with desirable adhesive properties vis-à-vis the virus.

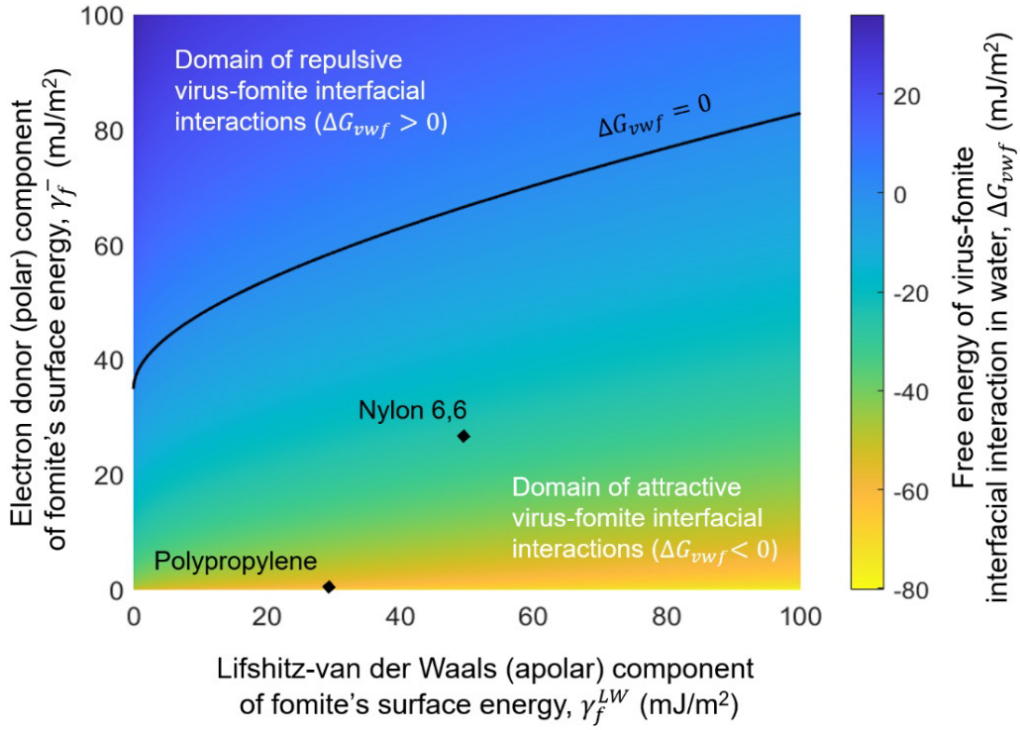

Figure 3. Free energy, ΔG_{vwf}, of interfacial interaction of HRSV with *monopolar* fomites (γ_f^+ = 0) in DI water. The solid line corresponds to ΔG_{vwf} = 0 (i. e. solution of eq. (16)).

[1] In his book "Interfacial Forces in Aqueous Media", van Oss pointed out that electron donor-only monopolar (γ_s^+ = 0) surfaces with γ_s^{LW} = 40 mJ·m^{-2} ("a typical value for most biological and many other organic materials") are hydrophilic when their γ_s^- is above 28.3 mJ·m^{-2}. In effect, this comment referred to a specific point on the ΔG_{sws}= 0 curve on a graph similar to Fig. 3 but drawn for ΔG_{sws}.

3.4 Virus adhesion to fomites: QCM-D measurements

3.4.1 Model of mass transfer in QCM-D chamber. Assumptions

Virus transport to the QCM-D sensor surface can be viewed a s a two-step process – long range transport from the bulk of the flow to the surface followed by a collision event, which may or may not result in an attachment. The attachment efficiency, α_{vf}, is defined as the probability that a collision results in attachment. The QCM-D part of the present work is designed to determined α_{vf} values so that they can be related to the energy of virus-fomite interactions. In the simple mass transfer model given by eq. (13), the long-range transport of a virus and short-range virus-fomite interactions are described by k and α_{vf}, respectively. The linearity of eq. (13) was tested and confirmed ($R^2 > 0.99$) in a subset of QCM-D tests with HAdV5 and SS (see SM, Fig. S3). Further, it was assumed that deposited virions formed a laterally homogeneous film. In reality, the deposited layer is laterally heterogeneous, consisting of discrete virions with a solvation shell contributing to the QCM-D signal to different extents at different coverages. The use of the Sauerbrey equation is justified, however, in view of the near-overlapping time dependencies of $\Delta f_n/n$ for different harmonics (see section 3.4.3) and a relatively weak dissipation signal $\Delta D_n/(\Delta f_n/n)$ << 4×10^{-7} Hz^{-1}) [41, 95].

3.4.2 Quantifying mass transfer in QCM-D chamber: Mass transfer coefficients for HAdV5 and HRSV and size of depositing virions.

Based on dm_v/dt values measured in tests with PP under conditions of attractive electrostatic interactions (i. e. assuming α_{vf} = 1; Fig. S9a, Fig. S9c), eq. (13) predicted the mass transfer coefficient, k, for HRSV and HAdV5 to be 5.97×10^{-9} (m/s) and 1.87×10^{-9} (m/s), respectively. The value of k for HAdV5 together with HAdV5 diffusion coefficient measured by DLS (section 3.1) can be used to estimate the effective thickness of the mass transfer boundary layer in the QCM-D chamber:

$$\delta \approx \frac{D}{k} \tag{17}$$

The thickness of boundary layer is defined by the hydrodynamics of the flow in the chamber and should be the same for both viruses. Given the very narrow size distribution for the HAdV5 stock (Fig. 1E) and, therefore, a more accurate D estimate for this virus, eq. (17) was applied to HAdV5 to predict $\delta \approx 2.3$ mm. This value of δ together with the value of k for HRSV can be used to predict the effective hydrodynamic diameter of HRSV based on Stokes-Einstein equation. Combining eq. (15) and eq. (17) gives:

$$d_h = \frac{k_B T}{3\pi\mu k\delta} \tag{18}$$

Eq. (18) predicts HRSV hydrodynamic diameter of 32 nm, which is an almost exact match to the higher peak in the size distribution for this virus (Fig. 1B). We conclude that the smaller size fraction of HRSV is the morphological subset of HRSV virions that

predominantly deposit on the QCM-D sensor surface. While the polydispersity of HRSV (Fig. 1B) confounds a direct application of size data in mass transfer calculations for this virus, the above analysis shows that QCM-D signal is due to the deposition of virions from the smaller size fraction of the HRSV population.

3.4.3 Virus deposition onto fomites. Virus-fomite attachment efficiency, α_{vf}.

Figure 4 shows a QCM-D dataset recorded in experiments on virus deposition from 150 mM NaCl solution. Representative QCM-D results (both frequency and dissipation signals) from tests with all virus-fomites pairs are given in SM (Figures S10 - S17). During the virus deposition stage, the dissipation signal increased monotonously, with a relatively constant deposition rate, dm_v/dt, indicating early stages of the deposition process, far from the jamming limit. Indeed, based on the areal mass density and virion size, the surface coverage was below 4 % for HRSV and below 1 % for HAdV.

Three additional observations in QCM-D tests require a commentary. First, changes in the QCM-D signal in response to changes of the background solution (from DI to 150 mM and back) were not immediate. The transient period is due to a finite retention time within the QCM-D chamber. The lower bound on the retention time in the tubing and the QCM-D chamber is ~ 1.5 min; the estimate considers QCM-D chamber as an ideal completely mixed flow reactor so that the actual retention time should be higher.

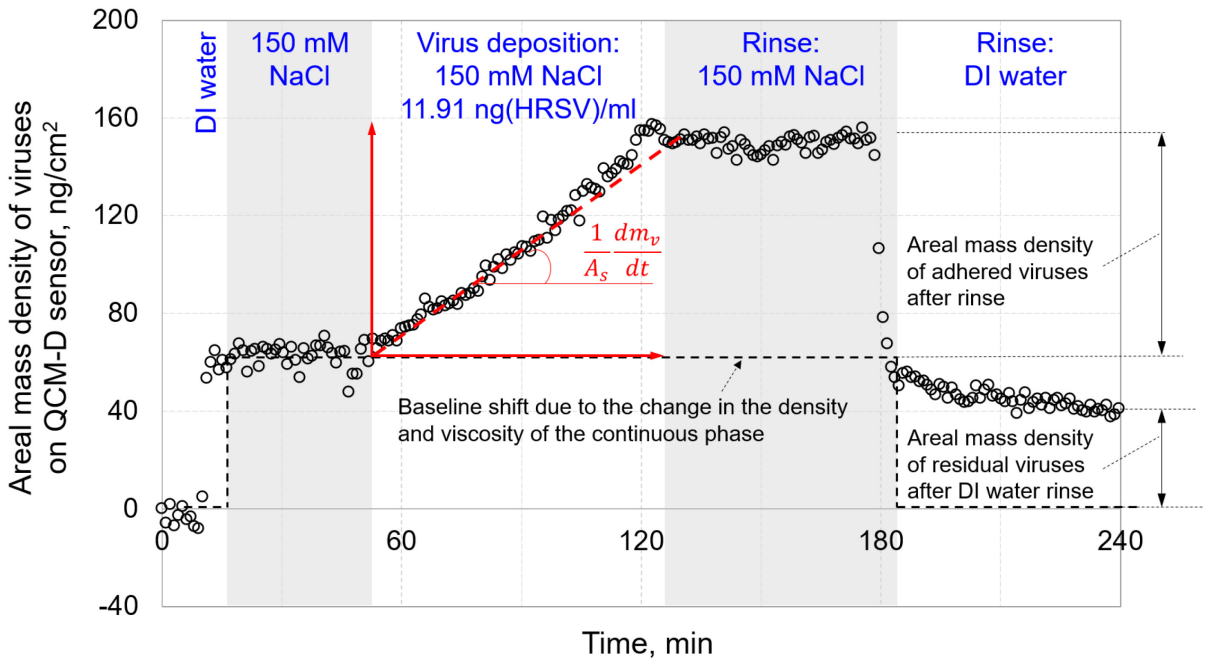

Figure 4. Example QCM-D data set: deposition of HRSV on stainless steel.

Representative QCM-D data for all virus-fomite pairs and deposition conditions are given in SM (Figures S10 – S17). All calculations based on the QCM-D data were performed using the signal for the 5th overtone (n = 5 in eq. (14)). The reason for choosing the 5th harmonic was that the signals for the 3rd and 1st harmonics were unstable, likely due to their high sensitivity to mounting stress caused by the O-rings holding the sensor within the QCM-D chamber [96].

Second, averaged over all 24 QCM-D experiments (8 virus-fomite pairs, triplicate tests), the frequency shift due to the change of the solution from DI water to 150 mM NaCl was 20.9 ± 4.0 Hz. This was smaller than the shift predicted by the Kanazawa-Gordon equation (64.6 Hz; see eq. (S1)) based on the density and viscosity of the two solutions

at 20 °C [97, 98]. The discrepancy may be due to a limited sensitivity of the sensors or a variation in the density of the quartz sensor. Third, the high reproducibility of dm_v/dt values for each condition indicated that the limited reuse of QCM-D sensors (for cleaning protocols see SM, section S4) had little impact on virus adhesion. This is consistent with results of t-testing, which showed that sensor surface energy, ΔG_{fwf}, remained stable (p > 0.1) after repeated usage-cleaning cycles (Tables S3 and S4 vs Table S2).

Figure 5 shows values of the attachment efficiency computed based on dm_v/dt slopes in QCM-D tests with various virus-fomite pairs. For both HAdV5 and HRSV, more favorable interfacial interaction (quantitatively expressed in terms of ΔG_{vwf}) corresponded to a higher probability of attachment. Remarkably, normalization by C_b (a step in the computation of α_{vf}), made the α_{vf} vs ΔG_{vwf} dependencies for both viruses collapse into one trend, pointing to the possibility of using of ΔG_{vwf} as a predictor of virus adhesion. Whether this result holds true for other viruses and fomites warrants further testing.

As described in section 2.5.1, the determination of α_{vf} relies on quantifying the mass transfer coefficient, k, which is based on tests performed under conditions of highly favorable virus-fomite interaction with α_{vf} = 1. To model this scenario, QCM-D tests were performed with polypropylene as the most hydrophobic of the four fomites (to maximize hydrophobic attraction U_{vwf}^{AB}), and under conditions when the electrostatic

interactions are favorable ($U_{vwf}^{EL} < 0$) and strongest. The latter conditions were achieved by a) adjusting pH to be within the pH range bracketed by the pI values of polypropylene and the virus in question (see SM, section S6) and b) switching to low ionic strength electrolyte (1 mM NaCl) to minimize screening of attractive electrostatic interactions.

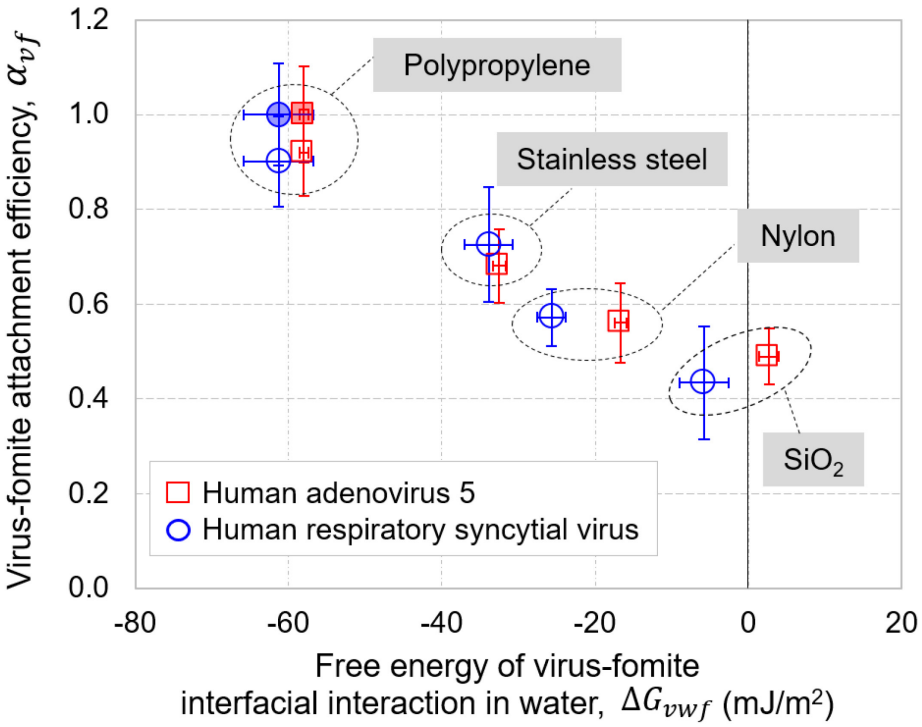

Figure 5. Virus-fomite attachment efficiency as a function of the free energy of virus-fomite interaction in water. Empty symbols correspond to tests with 150 mM NaCl electrolyte as the deposition solution. Filled symbols correspond to tests with virus deposition onto polypropylene from 1 mM NaCl at pH 4.1 for HAdV5 and at pH 3.8 for HRSV where virus-fomite electrostatic interaction is favorable and at its maximum absolute value. (See SM, section S6 for the algorithm used to select these pH values.)

Figure 6 gives examples of two QCM-D datasets that correspond to the least hydrophobic fomite-virus pair (silica and HAdV5 with ΔG_{fwf} of 15.7 and - 27.7 mJ·m^{-2}, respectively) and the most hydrophobic one (HRSV and PP with ΔG_{fwf} of - 40.2 and - 88.9 mJ·m^{-2}, respectively). As mentioned earlier, one simplification behind the presented approach is that the deposited layer is assumed to be laterally homogeneous. We note that this assumption provides a conservative estimate on the difference between hydrophilic and hydrophobic fomites in terms of their adhesiveness. The contribution of the solvent to the QCM-D signal should be higher for attached particles with a larger shell of associated solvent, especially at lower coverages [95], such as those (< 4%) that occurred in our QCM-D tests. Thus, we expect that due to the higher contribution of the solvation shell, the values of α_{vf} are overpredicted for more hydrophilic virion-fomite pairs; therefore, the contrast between PP and silica should be more pronounced than what is apparent from Fig. 5.

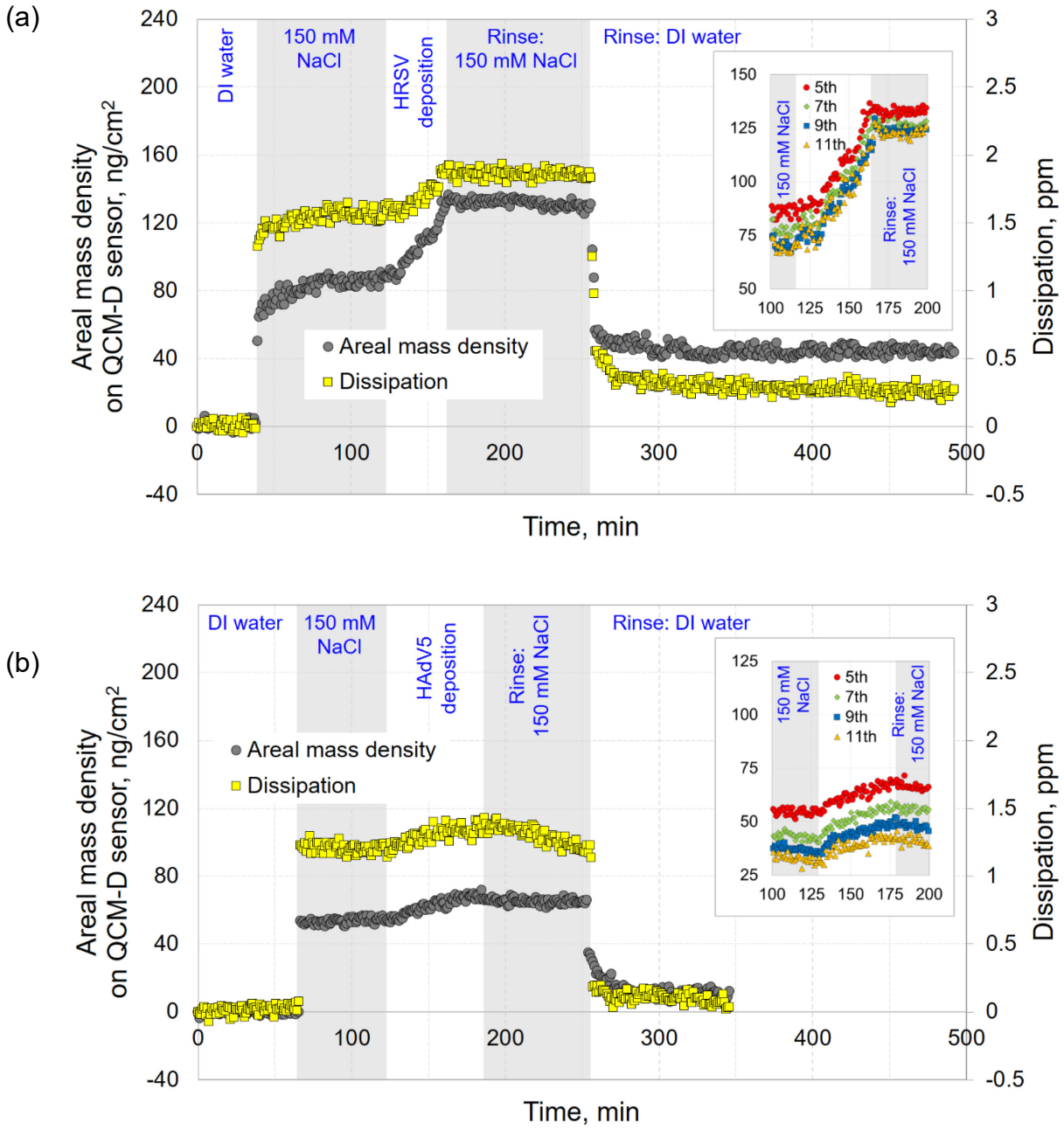

Figure 6. Mass and dissipation QCM-D data for the deposition of a) HRSV on polypropylene and b) HAdV5 on silica. Insets illustrate areal mass density values computed based on 5th, 7th, 9th, and 11th harmonics of the QCM-D signal.

3.5 XDLVO predictions

Virus properties required as inputs to XDLVO model included virus size as well as surface energy and ζ-potential of viruses and fomites. The ζ-potential of the four fomites as a function of pH was obtained from literature [36, 74, 75]. There was a significant variation in the reported values of ζ-potential of stainless steel [75, 99, 100] likely due to different degrees of passivation of the surface. While pure metals have very high surface energy, fast oxidation in air passivates the surface and minimizes its energy through the formation of a metal oxide bilayer. The passive film on the stainless steel surface consists of an inner sub-layer with segregated chromium oxide and an outer sublayer enriched in iron oxyhydroxide [101-103]. For XDLVO simulations, we adopted surface charge data reported by Hedberg et al. [75].

For both viruses, the XDLVO model predicted attractive interactions with nylon, SS and PP at all virus-fomite separation distances (Figures 7a, S5a, S5c, S6a, S7a, S7c, S8a) due to strong hydrophobic attraction. The XDLVO energy of interaction between silica and each of the two viruses featured a primary maximum and a secondary minimum. For HAdV5/silica (Fig. 7c), the corresponding energy values were 200 kT and - 3.0 kT; the reason for the very high primary energy barrier was the strong repulsive Lewis acid-base interaction between HAdV5 and silica ("hydration pressure") as indicated by the positive value of $\Delta G_{d_0}^{AB}$ (~7.9 mJ·m^{-2}; Table 2). For HRSV/silica (Fig. S8c), the primary maximum was much lower (21 kT) while the secondary minimum was shallower (– 2.3

kT). The repulsive electrostatic interaction between HRSV and silica results in slightly repulsive total interaction even though LW and AB interactions are both attractive ($\Delta G_{d_0}^{LW}$ = -5.5 J·m^{-2}, $\Delta G_{d_0}^{AB} \approx$ - 0.4 J·m^{-2}; Table 2). During DI water rinse, there was always an energy barrier for all virus-fomite pairs except for the condition of α_{vf} = 1. In XDLVO simulations describing the DI rinse, the ionic strength of the solution was assumed to be 10^{-5} M.

In XDLVO energy profiles corresponding to the conditions of DI water rinse (Fig. 7b, Fig 7d), the energy barriers were observed in all the cases at longer distance (> 5 nm) except for HAdV5/silica, where barrier was located at the distance of ~ 0.4 nm. The appearance of energy barriers is due to the increased importance of repulsive electrostatic interactions. In high ionic strength solution, the electrostatic interaction is limited due to the compression of the electric double layer, making the U_{vwf}^{EL} decrease much faster with distance. With the lowering of the ionic strength, this restriction disappears, making U_{vwf}^{EL} higher at longer distance. This is consistent with QCM-D results showing a much more effective removal of viruses when switching from 150 mM rinse to DI water rinse.

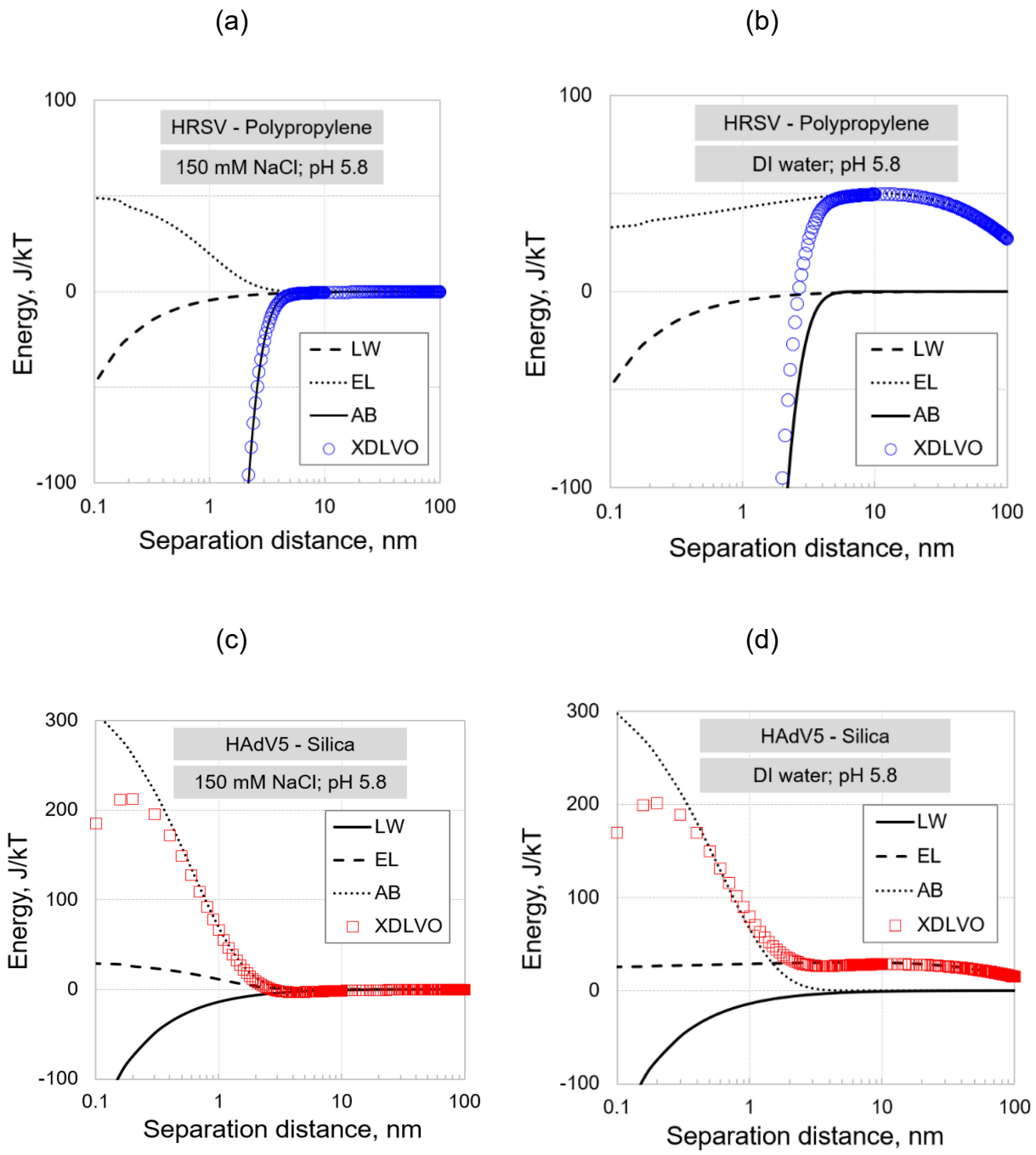

Figure 7. XDLVO total energy of interactions during virus deposition (a, c) and cleaning (b, d) stages of QCM-D experiments. The results are for HRSV interaction with polypropylene (a, b) and HAdV5 interaction with silica (c, d).

While outside of the scope of the present work, testing non-polar liquids as cleaning agents for virus removal is also of interest.

The XDLVO modeling complements interfacial energy analysis (Table 2) by providing insights into the relative importance of electrostatic interactions as a function of ionic strength. Accounting for classical DLVO (LW, EL) as well as polar (AB) interactions, the model predicts that at lower ionic strengths a solution with an appropriate pH deters adhesion and can help resuspend attached viruses. Separation distances that correspond to primary maxima (barriers for irreversible adhesion) and secondary minima (loci for possible reversible adhesion) correspond to a fraction of a virus diameter. Thus, for solution chemistries that discourage adhesion, a very minor disturbance in a virus' position at the surface may lead to detachment. While almost no removal of viruses was observed by flowing 150 mM NaCl solution after virus deposition, removal of 28.8% on average was possible after switching to DI water as the rinsing solution. These findings are also consistent with the results reported by Liu et al who employed SPR imaging to study adsorption of SARS-CoV-2 pseudovirus onto model surfaces [40]. Under conditions when the virus and the surface carried the charge of the same sign, adsorption was stronger at a higher ionic strength where the repulsive electrostatic interactions are screened out.

In general, anti-adhesion surfaces should have high positive value of the interfacial free energy of its interaction with a virus, ΔG_{vwf} (see Fig. 3). Consistent with XDLVO

modelling results, QCM-D data show that for both HAdV and HRSV, the efficiency of their attachment to fomites is correlated with ΔG_{vwf}. For a virus with known surface tension parameters, this knowledge can be used to select surfaces with as high ΔG_{vwf} as practically possible to deter virus adhesion. The proposed approach can also guide the selection of surface cleaning solutions and protocols. When the virus and surface carry electrical charges of the same sign, a cleaning solution with low ionic strength will allow for electrostatic repulsion. Whereas if the virus and surface are oppositely charged, cleaning solution with a high ionic strength can screed out attractive electrostatic interactions. Both strategies should promote virus detachment.

5. Conclusions

The present work considers interactions of two human enteric viruses – one enveloped (HRSV) and one non-enveloped (HAdV5) – with four fomites (silica, nylon, stainless steel, polypropylene). The selected fomites are tentatively identified as “archetypes” representing surfaces that are distinctly different in mechanisms of their interfacial interactions. The surfaces are typified on the basis of their surface energy components:

- Archetype 1 (e. g. silica) is characterized by a large electron donor component such that $\gamma_f^- \gg \gamma_f^+$. For these surfaces, hydration pressure can overcome water cohesion to result in an overall repulsion of viruses.

- Archetype 2 (e. g. nylon) is less polar than archetype 1 and has high dispersive component, γ_f^{LW}. A near-monopolar surface ($\gamma_f^+ \cong 0$), archetype 2 also has a smaller γ_f^-. As a result, the electron-donor attraction between archetype 2 and viruses is weaker than water cohesion leading to hydrophobic attraction that is further enhanced due to dispersive forces.
- Archetype 3 (e. g. stainless steel) has a substantial electron acceptor component such that $\gamma_f^+ \cong \gamma_f^-$. This gives stronger polar interactions with viruses (i. e. higher $\gamma_f^+\gamma_v^-$ and $\gamma_f^-\gamma_v^+$).
- Archetype 4 (e. g. polypropylene) is an apolar material ($\gamma_f^+ \cong 0$; $\gamma_f^- \cong 0$) with the dispersive component, γ_f^{LW}, close to that of water. Hydrophobic attraction is the dominant mechanism of virus interaction with such surfaces.

Areal mass density on the fomite surface is found to correlate with the free energy of virus-fomite interfacial interaction in water, ΔG_{vwf}. For both HAdV5 and HRSV, more negative ΔG_{vwf} values correspond to higher virus-fomite attachment efficiencies. Moreover, α_{vf} vs ΔG_{vwf} dependencies for HAdV5 and HRSV collapse into one trend pointing to the possibility of using ΔG_{vwf} as a predictor of virus adhesion. Virus deposition from 150 mM NaCl electrolyte is defined by polar interactions. Under conditions of low ionic strength, however, electrostatic forces emerge as a dominant interaction at a longer range.

Through the analysis of relative contributions of separate surface tension components to the energy of interfacial interaction, the study describes a possible approach to the selection of surfaces with desired adhesion properties. The methodology helps fill the knowledge gap on virus adhesion to fomites – an important component of models on virus transport and fate in built environments. The study can help guide screening and selection of materials that discourage virus adhesion, design of anti-adhesive surfaces, as well as development of surface cleaning solutions and protocols.

Acknowledgements

This material is based upon work supported in part by the U.S. National Science Foundation under Grant OISE-1952438 and in part by the Research Council of Norway under project #310074. We are grateful to Dr. Wei Zhang (Department of Plant, Soil and Microbial Sciences, Michigan State University) for making available the Malvern Zetasizer Nano-ZS instrument in his laboratory as well as to Dr. Irene Xagoraraki and Brijen Miyani (Department of Civil and Environmental Engineering, Michigan State University) for providing training on the procedures for RNA and DNA extraction.

Nomenclature

α_{vf}	virus-fomite attachment efficiency
γ_l^{LW}	Lifshitz-van der Waals component of the surface energy of probe liquid
γ_s^{LW}	Lifshitz-van der Waals component of the surface energy of solid
γ_w^{LW}	Lifshitz-van der Waals component of the surface energy of water
γ_l^+	electron acceptor component of the surface energy of probe liquid
γ_s^+	electron acceptor component of the surface energy of solid
γ_w^+	electron acceptor component of the surface energy of water
γ_l^-	electron donor component of the surface energy of probe liquid
γ_s^-	electron donor component of the surface energy of solid
γ_w^-	electron donor component of the surface energy of water
δ	effective diffusion distance
ε_r	relative dielectric permittivity of water
ε_0	dielectric permittivity of vacuum
ζ	ζ-potential
θ	contact angle
κ	inverse Debye screening length (also referred to as Hückel parameter)
λ	(=0.6 nm) the decay length for Lewis acid-base interaction in water
μ	dynamic viscosity
ψ_v	surface potential of a virus
ψ_f	surface potential of a fomite

A	Hamaker constant
A_s	surface area of the QCM sensor
a	virus radius
C	QCM sensor mass sensitivity constant
C_b	virus concentration in the bulk of the flow
C_s	virus concentration at the sensor surface
D	diffusion coefficient
d	virus-fomite minimal separation distance
d_h	hydrodynamic diameter
d_0	minimum separation distance due to Born repulsion
k	mass transfer coefficient
k_B	Boltzmann's constant
E_{max}	primary maximum in the total XDLVO energy of interaction
E_{min}	secondary minimum in the total XDLVO energy of interaction
Δf	QCM vibration frequency shift
ΔG_{fwf}	free energy of interfacial interaction of two identical fomites in water
ΔG_{sws}	free energy of interfacial interaction of two identical solids in water
ΔG_{vwv}	free energy of interfacial interaction of two identical viruses in water
ΔG_{vwf}	free energy of virus-fomite interfacial interaction in water
j_m	mass flux of virus towards the QCM sensor

m	areal mass density
n	QCM vibration overtone number
U_{slv}^{XDLVO}	total XDLVO energy of interaction between a sphere and a plate
U_{vwf}^{LW}	energy of Lifshitz-van der Waals interaction between a sphere and a plate
U_{vwf}^{EL}	energy of electrostatic interaction between a sphere and a plate
U_{vwf}^{AB}	energy of Lewis acid-base interaction between a sphere and a plate
T	absolute temperature

References

[1] N. Castaño, S. Cordts, M.K. Jalil, K. Zhang, S. Koppaka, A. Bick, R. Paul, S.K. Tang, Fomite transmission, physicochemical origin of virus–surface interactions, and disinfection strategies for enveloped viruses with applications to SARS-CoV-2, ACS Omega (2021). https://doi.org/10.1021/acsomega.0c06335

[2] S.A. Boone, C.P. Gerba, Significance of fomites in the spread of respiratory and enteric viral disease, Appl. Environ. Microbiol. 73(6) (2007) 1687-1696. https://doi.org/10.1128/aem.02051-06

[3] B. Stephens, P. Azimi, M.S. Thoemmes, M. Heidarinejad, J.G. Allen, J.A. Gilbert, Microbial exchange via fomites and implications for human health, Curr. Poll. Rep. (2019) 1-16. https://doi.org/10.1007/s40726-019-00123-6

[4] F. Pancic, D.C. Carpenter, P.E. Came, Role of infectious secretions in the transmission of rhinovirus. , J. Clin. Microbiol. 12 (1980) 567-571. https://dx.doi.org/10.1128/JCM.12.4.567-571.1980

[5] A.A. Chughtai, S. Stelzer-Braid, W. Rawlinson, G. Pontivivo, Q. Wang, Y. Pan, D. Zhang, Y. Zhang, L. Li, C.R. MacIntyre, Contamination by respiratory viruses on outer surface of medical masks used by hospital healthcare workers, BMC Infect. Dis. 19(1) (2019). https://doi.org/10.1186/s12879-019-4109-x

[6] M.Z. Hassan, K. Sturm-Ramirez, M.Z. Rahman, K. Hossain, M.A. Aleem, M.U. Bhuiyan, M.M. Islam, M. Rahman, E.S. Gurley, Contamination of hospital surfaces with respiratory pathogens in Bangladesh, PLOS One 14(10) (2019) e0224065. https://doi.org/10.1371/journal.pone.0224065

[7] E.K. Kurgat, J.D. Sexton, F. Garavito, A. Reynolds, R.D. Contreras, C.P. Gerba, R.A. Leslie, S.L. Edmonds-Wilson, K.A. Reynolds, Impact of a hygiene intervention on virus spread in an office building, Int. J. Hyg. Environ. Health 222(3) (2019) 479-485. https://doi.org/10.1016/j.ijheh.2019.01.001

[8] J.M.L. Brotherton, V.C. Delpech, G.L. Gilbert, S. Hatzi, P.D. Paraskevopoulos, J.M. McAnulty, A large outbreak of influenza A and B on a cruise ship causing widespread morbidity, Epidemiol. Infect. 130(2) (2003) 263-271. https://doi.org/10.1017/s0950268802008166

[9] S. Xiao, Y. Li, T.-W. Wong, D.S.C. Hui, Role of fomites in SARS transmission during the largest hospital outbreak in Hong Kong, PLOS One 12(7) (2017). https://doi.org/10.1371/journal.pone.0181558

[10] S.F. Dowell, J.M. Simmerman, D.D. Erdman, J.-S.J. Wu, A. Chaovavanich, M. Javadi, J.-Y. Yang, L.J. Anderson, S. Tong, M.S. Ho, Severe acute respiratory syndrome coronavirus on hospital surfaces, Clin. Infect. Dis. 39(5) (2004) 652-657. https://doi.org/10.1086/422652

[11] A.J. Prussin II, J.A. Belser, W. Bischoff, S.T. Kelley, K. Lin, W.G. Lindsley, J.P. Nshimyimana, M. Schuit, Z. Wu, K. Bibby, L.C. Marr, Viruses in the Built Environment (VIBE) meeting report, Microbiome 8 (2020) 1. https://doi.org/10.1186/s40168-019-0777-4

[12] H. Sakaguchi, K. Wada, J. Kajioka, M. Watanabe, R. Nakano, T. Hirose, H. Ohta, Y. Aizawa, Maintenance of influenza virus infectivity on the surfaces of personal protective equipment and clothing used in healthcare settings, Environmental Health and Preventive Medicine 15(6) (2010) 344-349. https://doi.org/10.1007/s12199-010-0149-y

[13] F. Cui, X. Geng, O. Zervaki, D.D. Dionysiou, J. Katz, S.-J. Haig, M. Boufadel, Transport and fate of virus-laden particles in a supermarket: Recommendations for risk reduction of COVID-19 spreading, J. Environ. Eng. 147(4) (2021) 04021007. https://doi.org/10.1061/(ASCE)EE.1943-7870.0001870

[14] A.K. Pitol, T.R. Julian, Community transmission of SARS-CoV-2 by fomites: Risks and risk reduction strategies, Environ. Sci. Technol. Lett. 8 (2021) 263−269. https://dx.doi.org/10.1021/acs.estlett.0c00966

[15] A. Meiksin, Dynamics of COVID-19 transmission including indirect transmission mechanisms: A mathematical analysis, Epidemiol. Infect. 148 (2020) e257. https://doi.org/10.1017/s0950268820002563

[16] L. Owen, K. Laird, The role of textiles as fomites in the healthcare environment: a review of the infection control risk, PeerJ 8 (2020) e9790. https://doi.org/10.7717/peerj.9790

[17] A. Brlek, Š. Vidovič, S. Vuzem, K. Turk, Z. Simonović, Possible indirect transmission of COVID-19 at a squash court, Slovenia, March 2020: Case report, Epidemiol. Infect. 148 (2020) e120. https://doi.org/10.1017/s0950268820001326

[18] Z. Zhang, L. Zhang, Y. Wang, COVID‐19 indirect contact transmission through the oral mucosa must not be ignored, J. Oral Pathology Med. 49(5) (2020) 450-451. https://doi.org/10.1111/jop.13019

[19] T. Yamagishi, M. Ohnishi, N. Matsunaga, K. Kakimoto, H. Kamiya, K. Okamoto, M. Suzuki, Y. Gu, M. Sakaguchi, T. Tajima, S. Takaya, N. Ohmagari, M. Takeda, S. Matsuyama, K. Shirato, N. Nao, H. Hasegawa, T. Kageyam, I. Takayama, S. Saito, K. Wada, R. Fujita, H. Saito, K. Okinaka, M. Griffith, A.E. Parry, B. Barnetson, J. Leonard, Environmental sampling for severe acute respiratory syndrome coronavirus 2 during a COVID-19 outbreak on the Diamond Princess cruise ship, J. Infect. Dis. 222(7) (2020) 1098-1102. https://doi.org/10.1093/infdis/jiaa437

[20] S.W.X. Ong, Y.K. Tan, P.Y. Chia, T.H. Lee, O.T. Ng, M.S.Y. Wong, K. Marimuthu, Air, surface environmental, and personal protective equipment contamination by severe acute respiratory syndrome coronavirus 2 (SARS-CoV-2) from a symptomatic patient, JAMA 323(16) (2020) 1610-1612. https://doi.org/10.1001/jama.2020.3227

[21] B. Pastorino, F. Touret, M. Gilles, X. de Lamballerie, R. Charrel, Prolonged infectivity of SARS-CoV-2 in fomites, Emerg. Infect. Dis. 26(9) (2020) 2256-2257. https://dx.doi.org/10.3201/eid2609.201788

[22] Z.-D. Guo, Z.-Y. Wang, S.-F. Zhang, X. Li, L. Li, C. Li, Y. Cui, R.-B. Fu, Y.-Z. Dong, X.-Y. Chi, Aerosol and surface distribution of severe acute respiratory syndrome coronavirus 2 in hospital wards, Wuhan, China, 2020, Emerg. Infect. Dis. 26(7) (2020) 1583-1591. https://doi.org/10.3201/eid2607.200885

[23] P.Y. Chia, K.K. Coleman, Y.K. Tan, S.W.X. Ong, M. Gum, S.K. Lau, X.F. Lim, A.S. Lim, S. Sutjipto, P.H. Lee, Detection of air and surface contamination by SARS-CoV-2 in hospital rooms of infected patients, Nature Comm. 11(1) (2020) 1-7. https://doi.org/10.1038/s41467-020-16670-2

[24] N. Van Doremalen, T. Bushmaker, D.H. Morris, M.G. Holbrook, A. Gamble, B.N. Williamson, A. Tamin, J.L. Harcourt, N.J. Thornburg, S.I. Gerber, Aerosol and surface stability of SARS-CoV-2 as compared with SARS-CoV-1, New Engl. J. Med. 382(16) (2020) 1564-1567. https://doi.org/10.1056/NEJMc2004973

[25] Transmission of SARS-CoV-2: implications for infection prevention precautions: Scientific Brief, 09 July 2020, World Health Organization, 2020.

[26] A.P. Harvey, E.R. Fuhrmeister, M. Cantrell, A.K. Pitol, J.M. Swarthout, J.E. Powers, M.L. Nadimpalli, T.R. Julian, A.J. Pickering, Longitudinal monitoring of SARS-CoV-2

RNA on high-touch surfaces in a community setting, Environ. Sci. Technol. Lett. 8(2) (2021) 168-175. https://doi.org/10.1021/acs.estlett.0c00875

[27] F.X. Abad, C. Villena, S. Guix, S. Caballero, R.M. Pintó, A. Bosch, Potential role of fomites in the vehicular transmission of human astroviruses, Appl. Environ. Microbiol. 67(9) (2001) 3904-3907. http://dx.doi.org/10.1128/AEM.67.9.3904-3907.2001

[28] A. Kramer, I. Schwebke, G. Kampf, How long do nosocomial pathogens persist on inanimate surfaces? A systematic review, BMC Infect. Dis. 6(1) (2006) 130. https://doi.org/10.1186/1471-2334-6-130

[29] A. Chabrelie, J. Mitchell, J. Rose, D. Charbonneau, Y. Ishida, Evaluation of the influenza risk reduction from antimicrobial spray application on porous surfaces, Risk Anal. 38(7) (2018) 1502-1517. https://doi.org/10.1111/risa.12952

[30] B. Killingley, J. Nguyen‐Van‐Tam, Routes of influenza transmission, Influenza Other Resp. 7 (2013) 42-51. https://doi.org/10.1111/irv.12080

[31] R.A. Canales, K.A. Reynolds, A.M. Wilson, S.L. Fankem, M.H. Weir, J.B. Rose, S. Abd-Elmaksoud, C.P. Gerba, Modeling the role of fomites in a norovirus outbreak, J. Occup. Environ. Hyg. 16(1) (2019) 16-26. https://doi.org/10.1080/15459624.2018.1531131

[32] E.L. Jones, A. Kramer, M. Gaither, C.P. Gerba, Role of fomite contamination during an outbreak of norovirus on houseboats, Int. J. Environ. Health Res. 17(2) (2007) 123-131. https://doi.org/10.1080/09603120701219394

[33] M.O. Aydogdu, E. Altun, E. Chung, G. Ren, S. Homer-Vanniasinkam, B. Chen, M. Edirisinghe, Surface interactions and viability of coronaviruses, J. R. Soc. Interface 18 (2021). https://doi.org/10.1098/rsif.2020.0798

[34] B. Michen, F. Meder, A. Rust, J. Fritsch, C. Aneziris, T. Graule, Virus removal in ceramic depth filters based on diatomaceous earth, Environ. Sci. Technol. 46(2) (2012) 1170-1177. https://doi.org/10.1021/es2030565

[35] J.-A. Park, S.-B. Kim, DLVO and XDLVO calculations for bacteriophage MS2 adhesion to iron oxide particles, J. Contam. Hydrol. 181 (2015) 131-140. https://doi.org/10.1016/j.jconhyd.2015.01.005

[36] X. Wang, R. Şengür-Taşdemir, İ. Koyuncu, V.V. Tarabara, Lip balm drying promotes virus attachment: Characterization of lip balm coatings and XDLVO modeling, J. Colloid Interface Sci. 581 (2021) 884-894. https://doi.org/10.1016/j.jcis.2020.07.143

[37] I. Samandoulgou, I. Fliss, J. Jean, Adhesion of norovirus to surfaces: Contribution of thermodynamic and molecular properties using virus-like particles, Food Environ. Virol. (2021). https://doi.org/10.1007/s12560-021-09471-3

[38] H.T.T. Dang, V.V. Tarabara, Virus deposition onto polyelectrolyte-coated surfaces: A study with bacteriophage MS2, J. Colloid Interface Sci. 540 (2019) 155-166. https://doi.org/10.1016/j.jcis.2018.12.107

[39] K. Wong, B. Mukherjee, A.M. Kahler, R. Zepp, M. Molina, Influence of inorganic ions on aggregation and adsorption behaviors of human adenovirus, Environ. Sci. Technol. 46(20) (2012) 11145-11153. https://doi.org/10.1021/es3028764

[40] Y.-N. Liu, Z.-T. Lv, S.-Y. Yang, X.-W. Liu, Optical tracking of the interfacial dynamics of single SARS-CoV-2 pseudoviruses, Environ. Sci. Technol. 55 (2021) 4115−4122. https://dx.doi.org/10.1021/acs.est.0c06962

[41] A. Armanious, M. Aeppli, R. Jacak, D. Refardt, T. Sigstam, T. Kohn, M. Sander, Viruses at solid-water interfaces: a systematic assessment of interactions driving adsorption, Environ. Sci. Technol. 50(2) (2015) 732-743. https://doi.org/10.1021/acs.est.5b04644

[42] X.L. Zhou, Y. Yang, S. Wang, X.W. Liu, Surface plasmon resonance microscopy: From single-molecule sensing to single-cell imaging, Angew. Chem., Int. Ed. 59(5) (2020) 1776−1785. https://doi.org/10.1002/anie.201908806

[43] B. Yuan, M. Pham, T.H. Nguyen, Deposition kinetics of bacteriophage MS2 on a silica surface coated with natural organic matter in a radial stagnation point flow cell, Environ. Sci. Technol. 42(20) (2008) 7628-7633. https://doi.org/10.1021/es801003s

[44] M. Pham, E.A. Mintz, T.H. Nguyen, Deposition kinetics of bacteriophage MS2 to natural organic matter: Role of divalent cations, J. Colloid Interface Sci. 338(1) (2009) 1-9. https://doi.org/10.1016/j.jcis.2009.06.025

[45] H.T.T. Dang, V.V. Tarabara, Attachment of human adenovirus onto household paints, Colloids Surf. B 204 (2021). https://doi.org/10.1016/j.colsurfb.2021.111812

[46] X. Huang, J. Xu, H.-F. Ji, G. Li, H. Chen, Quartz crystal microbalance based biosensor for rapid and sensitive detection of maize chlorotic mottle virus, Anal. Methods 6(13) (2014) 4530-4536. https://doi.org/10.1039/C4AY00292J

[47] C.J. Van Oss, Interfacial forces in aqueous media, CRC Press, 2006.

[48] G.R. Nemerow, P.L. Stewart, V.S. Reddy, Structure of human adenovirus, Curr. Opin. Virol. 2(2) (2012) 115-121. https://doi.org/10.1016/j.coviro.2011.12.008

[49] C. San Martín, Latest insights on adenovirus structure and assembly, Viruses 4(5) (2012) 847-877. https://doi.org/10.3390/v4050847

[50] K. Sirikanchana, J.L. Shisler, B.J. Marinas, Effect of exposure to UV-C irradiation and monochloramine on adenovirus serotype 2 early protein expression and DNA replication, Appl. Environ. Microbiol. 74(12) (2008) 3774-3782. https://doi.org/10.1128/aem.02049-07

[51] S. Jing, J. Zhang, M. Cao, M. Liu, Y. Yan, S. Zhao, N. Cao, J. Ou, K. Ma, X. Cai, Household transmission of human adenovirus type 55 in case of fatal acute respiratory disease, Emerg. Infect. Dis. 25(9) (2019) 1756. https://doi.org/10.3201/eid2509.181937

[52] G. La Rosa, M. Fratini, S.D. Libera, M. Iaconelli, M. Muscillo, Viral infections acquired indoors through airborne, droplet or contact transmission, Ann. Ist. Super. Sanità 49 (2013) 124-132. https://doi.org/10.4415/ANN_13_02_03

[53] L. Liljeroos, M.A. Krzyzaniak, A. Helenius, S.J. Butcher, Architecture of respiratory syncytial virus revealed by electron cryotomography, PNAS 110(27) (2013) 11133-11138. https://doi.org/10.1073/pnas.1309070110

[54] A.R. Falsey, E.E. Walsh, Respiratory syncytial virus infection in adults, Clin. Microbiol. Rev. 13(3) (2000) 371-384. https://doi.org/10.1128/CMR.13.3.371

[55] C.B. Hall, R.G. Douglas Jr, Modes of transmission of respiratory syncytial virus, J. Pediatr. 99(1) (1981) 100-103. https://doi.org/10.1016/S0022-3476(81)80969-9

[56] C.B. Hall, R.G. Douglas Jr, J.M. Geiman, Possible transmission by fomites of respiratory syncytial virus, J. Infect. Dis. 141(1) (1980) 98-102. https://doi.org/10.1093/infdis/141.1.98

[57] E.P. Vejerano, L.C. Marr, Physico-chemical characteristics of evaporating respiratory fluid droplets, J. R. Soc. Interface 15(139) (2018) 20170939. https://doi.org/10.1098/rsif.2017.0939

[58] B.K. Walsh, D.J. Mackey, T. Pajewski, Y. Yu, B.M. Gaston, J.F. Hunt, Exhaled-breath condensate pH can be safely and continuously monitored in mechanically ventilated patients, Respir. Care 51(10) (2006) 1125-1131.

[59] R.M. Effros, K.W. Hoagland, M. Bosbous, D. Castillo, B. Foss, M. Dunning, M. Gare, W. Lin, F. Sun, Dilution of respiratory solutes in exhaled condensates, Am. J. Respir. Crit. Care Med. 165(5) (2002) 663-9. https://doi.org/10.1164/ajrccm.165.5.2101018

[60] ATCC Product Sheet. Human adenovirus 5 (ATCC® VR1516™).

[61] ATCC Certificate of Analysis. Adenovirus type 5 Reference Material.

[62] ATCC Product Information Sheet for VR-1516™.

[63] ATCC Product Sheet. Human respiratory syncytial virus, High titer (ATCC® VR-26PQ™).

[64] ATCC Certificate of Analysis. Human respiratory syncytial virus, High titer (Strain: Long).

[65] Z. Ke, R. Dillard, T. Chirkova, F. Leon, C. Stobart, C. Hampton, J. Strauss, D. Rajan, C. Rostad, J. Taylor, H. Yi, R. Shah, M. Jin, T. Hartert, R. Peebles, B. Graham, M. Moore, L. Anderson, E. Wright, The morphology and assembly of respiratory syncytial virus revealed by cryo-electron tomography, Viruses 10(8) (2018) 446. https://doi.org/10.3390/v10080446

[66] C. Griffiths, S.J. Drews, D.J. Marchant, Respiratory syncytial virus: infection, detection, and new options for prevention and treatment, Clin. Microbiol. Rev. 30(1) (2017) 277-319. https://doi.org/10.1128/cmr.00010-16

[67] G. Kiss, J.M. Holl, G.M. Williams, E. Alonas, D. Vanover, A.W. Lifland, M. Gudheti, R.C. Guerrero-Ferreira, V. Nair, H. Yi, B.S. Graham, P.J. Santangelo, E.R. Wright, Structural analysis of respiratory syncytial virus reveals the position of M2-1 between the matrix protein and the ribonucleoprotein complex, J. Virol. 88(13) (2014) 7602-7617. https://doi.org/10.1128/jvi.00256-14

[68] C.J. van Oss, M.K. Chaudhury, R.J. Good, Interfacial Lifshitz-van der Waals and polar interactions in macroscopic systems, Chem. Rev. 88(6) (1988) 927-941. https://doi.org/10.1021/cr00088a006

[69] M.E. Schrader, Young-Dupre revisited, Langmuir 11 (1995) 3585-3589. https://doi.org/10.1021/la00009a049

[70] H. Shi, V.V. Tarabara, Charge, size distribution and hydrophobicity of viruses: Effect of propagation and purification methods, J. Virol. Methods 256 (2018) 123-132. https://doi.org/10.1016/j.jviromet.2018.02.008

[71] E.M.V. Hoek, G.K. Agarwal, Extended DLVO interactions between spherical particles and rough surfaces, J. Colloid Interface Sci. 298 (2006) 50-58. https://doi.org/10.1016/j.jcis.2005.12.031

[72] X. Huang, S. Bhattacharjee, E.M.V. Hoek, Is surface roughness a "Scapegoat" or a primary factor when defining particle - substrate interactions?, Langmuir 26 (2010) 2528-2537. https://doi.org/10.1021/la9028113

[73] Nanoscience Instruments (personal communication).

[74] L.F. Zemljič, O. Plohl, A. Vesel, T. Luxbacher, S. Potrč, Physicochemical characterization of packaging foils coated by chitosan and polyphenols colloidal formulations, Int. J. Mol. Sci. 21(2) (2020) 495. https://doi.org/10.3390/ijms21020495

[75] Y. Hedberg, X. Wang, J. Hedberg, M. Lundin, E. Blomberg, I.O. Wallinder, Surface-protein interactions on different stainless steel grades: effects of protein adsorption, surface changes and metal release, J. Mater. Sci.: Mater. Med. 24(4) (2013) 1015-1033. https://doi.org/10.1007/s10856-013-4859-8

[76] X. Zhang, R. Bai, Adsorption behavior of humic acid onto polypyrrole-coated nylon 6, 6 granules, J. Mater. Chem. 12(9) (2002) 2733-2739. https://doi.org/10.1039/B201364A

[77] L. Graetz, Ueber die Wärmeleitungsfähigkeit von Flüssigkeiten, Annalen der Physik 254 (79) (1882) 79-94. https://doi.org/10.1002/andp.18822540106

[78] W.M. Deen, Analysis of Transport Phenomena, Oxford University Press, 1998.

[79] G. Sauerbrey, Verwendung von Schwingquarzen zur Wägung dünner Schichten und zur Mikrowägung, Zeitschrift für Physik 155(2) (1959) 206-222. https://doi.org/10.1007/BF01337937

[80] J.-L. Putaux, A. Buléon, R. Borsali, H. Chanzy, Ultrastructural aspects of phytoglycogen from cryo-transmission electron microscopy and quasi-elastic light scattering data, Int. J. Biol. Macromol. 26(2) (1999) 145-150. https://doi.org/10.1016/S0141-8130(99)00076-8

[81] H. Shi, I. Xagoraraki, K.N. Parent, M.L. Bruening, V.V. Tarabara, Elution is a critical step for recovering human adenovirus 40 from tap water and surface water by cross-flow ultrafiltration, Appl. Environ. Microbiol. 82(16) (2016) 4982. https://doi.org/10.1128/AEM.00870-16

[82] H. Ohshima, A simple expression for Henry's function for the retardation effect in electrophoresis of spherical colloidal particles, J. Colloid Interface Sci. 168(1) (1994) 269-271. https://doi.org/10.1006/jcis.1994.1419

[83] H. Fischer, J.H. Widdicombe, Mechanisms of acid and base secretion by the airway epithelium, J. Membr. Biol. 211(3) (2006) 139-150. https://doi.org/10.1007/s00232-006-0861-0

[84] N. Albinana-Gimenez, P. Clemente-Casares, B. Calgua, J.M. Huguet, S. Courtois, R. Girones, Comparison of methods for concentrating human adenoviruses, polyomavirus JC and noroviruses in source waters and drinking water using quantitative PCR, J. Virol. Methods 158(1) (2009) 104-109. http://dx.doi.org/10.1016/j.jviromet.2009.02.004

[85] C. Gibbons, R. Rodriguez, L. Tallon, M. Sobsey, Evaluation of positively charged alumina nanofibre cartridge filters for the primary concentration of noroviruses, adenoviruses and male-specific coliphages from seawater, J. Appl. Microbiol. 109(2) (2010) 635-641. https://doi.org/10.1111/j.1365-2672.2010.04691.x

[86] H. Shi, E.V. Pasco, V.V. Tarabara, Membrane-based methods of virus concentration from water: a review of process parameters and their effects on virus recovery, Environ. Sci. Water Res. Technol. 3 (2017) 778-792. https://doi.org/10.1039/C7EW00016B

[87] G. Hwang, C.-H. Lee, I.-S. Ahn, B.J. Mhin, Determination of reliable Lewis acid-base surface tension components of a solid in LW-AB approach, J. Ind. Eng. Chem. 17 (2011) 125-129. https://doi.org/10.1016/j.jiec.2010.12.009

[88] E. McCafferty, Acid-base effects in polymer adhesion at metal surfaces, J. Adhes. Sci. Technol. 16(3) (2002) 239-255. https://doi.org/10.1163/156856102317295478

[89] L.-K. Chau, M.D. Porter, Surface isoelectric point of evaporated silver films: Determination by contact angle titration, J. Colloid Interface Sci. 145(1) (1991) 283−286. https://doi.org/10.1016/0021-9797(91)90121-N

[90] M.F. Cuddy, A.R. Poda, L.N. Brantley, Determination of isoelectric points and the role of pH for common quartz crystal microbalance sensors, ACS Appl. Mater. Interf. 5 (2013) 3514−3518. https://doi.org/10.1021/am400909g

[91] E. Virga, E. Spruijt, W.M. de Vos, P.M. Biesheuvel, Wettability of amphoteric surfaces: The effect of pH and ionic strength on surface ionization and wetting, Langmuir 34 (2018) 15174−15180. https://doi.org/10.1021/acs.langmuir.8b02875

[92] P.K. Weissenborn, R.J. Pugh, Surface tension of aqueous solutions of electrolytes: Relationship with ion hydration, oxygen solubility, and bubble coalescence, J. Colloid Interface Sci. 184 (1996) 550-563. https://doi.org/10.1006/jcis.1996.0651

[93] A.J. Kinloch, Adhesion and Adhesives: Science and Technology, Springer, 1987.

[94] C.J. van Oss, M.K. Chaudhury, R.J. Good, Monopolar surfaces, Adv. Colloid Interface Sci. 28 (1987) 35-64. https://doi-org.proxy1.cl.msu.edu/10.1016/0001-8686(87)80008-8

[95] I. Reviakine, D. Johannsmann, R.P. Richter, Hearing what you cannot see and visualizing what you hear: Interpreting quartz crystal microbalance data from solvated interfaces, Anal. Chem. 83(23) (2011) 8838-8848. https://doi.org/10.1021/ac201778h

[96] M. Rodal, How are QCM results influenced by the lateral distribution of the measured layer? Surface Science Blog, Biolin Scientific, 2019. https://www.biolinscientific.com/blog/how-are-qcm-results-influenced-by-the-lateral-distribution-of-the-measured-layer. (Accessed April 9 2021).

[97] K.K. Kanazawa, J.G. Gordon, Frequency of a quartz microbalance in contact with liquid, Anal. Chem. 57(8) (1985) 1770-1771. https://doi.org/10.1021/ac00285a062

[98] K.K. Kanazawa, J.G. Gordon, The oscillation frequency of a quartz resonator in contact with liquid, Anal. Chim. Acta 175 (1985) 99-105. https://doi.org/10.1016/S0003-2670(00)82721-X

[99] L. Boulangé-Petermann, A. Doren, B. Baroux, M.-N. Bellon-Fontaine, Zeta potential measurements on passive metals, J. Colloid Interface Sci. 171(1) (1995) 179-186. https://doi.org/10.1006/jcis.1995.1165

[100] S. Wu, S. Altenried, A. Zogg, F. Zuber, K. Maniura-Weber, Q. Ren, Role of the surface nanoscale roughness of stainless steel on bacterial adhesion and microcolony formation, ACS Omega 3(6) (2018) 6456-6464. https://doi.org/10.1021/acsomega.8b00769

[101] G. Okamoto, Passive film of 18-8 stainless steel structure and its function, Corrosion Sci. 13 (1973) 471-489. https://doi.org/10.1016/0010-938X(73)90031-0

[102] N. Sato, M. Cohen, The kinetics of anodic oxidation of iron in neutral solution: II The initial stages, J. Electrochem. Soc. 111 (1964) 512-522. https://doi.org/10.1149/1.2426171

[103] L. Boulange-Petermann, C. Jullien, P.E. Dubois , T. Benezech, C. Faille, Influence of surface chemistry on the hygienic status of industrial stainless steel, Biofouling 20(1) (2004) 25-33. https://doi.org/10.1080/08927010410001655542